ACS OMEGA

http://pubs.acs.org/journal/acsodf

Article

Anticorrosion Evaluation of Novel Water-Soluble Schiff Base Molecules for C1018 Steel in CO_2-Saturated Brine by Computational and Experimental Methodologies

Hany M. Abd El-Lateef,* Wafaa M. Abd El-Monem Nasr,* Mai M. Khalaf, Adila E. Mohamed, Mohamed Nageeb Rashed, and Mohamed Shaker S. Adam

Cite This: *ACS Omega* 2023, 8, 11512−11535

Read Online

ACCESS | Metrics & More | Article Recommendations | Supporting Information

ABSTRACT: In this work, three different derivatives of Schiff base, as mono- and di-Schiff bases, were successfully synthesized by the facile condensation of 2-aminopyridine, *o*-phenylenediamine, or 4-chloro-*o*-phenylenediamine with sodium salicylaldehyde-5-sulfonate (H1, H2, and H3, respectively). A combination of theoretical and practical studies was accomplished on the corrosion mitigation effect of the prepared Schiff base derivatives on C1018 steel in CO_2-saturated 3.5% NaCl solution. The corrosion inhibition effect of the synthesized Schiff base molecules was studied by electrochemical impedance spectroscopy (EIS) and potentiodynamic polarization (PDP) methods. The outcomes exhibited that Schiff base derivatives have an outstanding corrosion inhibition effect on carbon steel at particularly low concentrations in sweet conditions. The outcomes showed that Schiff base derivatives exhibited a satisfactory inhibition efficiency of 96.5% (H1), 97.7% (H2), and 98.1% (H3) with a dosage of 0.5 mM at 323 K. SEM/EDX analysis confirms the adsorbed inhibitor film's formation on the metal surface. The polarization plots indicate that the studied compounds behaved as inhibitors of the mixed type according to the isotherm model of Langmuir. The computational inspections (MD simulations and DFT calculations) display a good correlation with the investigational findings. The outcomes could be applied to assess the efficiency of the inhibiting agents in the gas and oil industry.

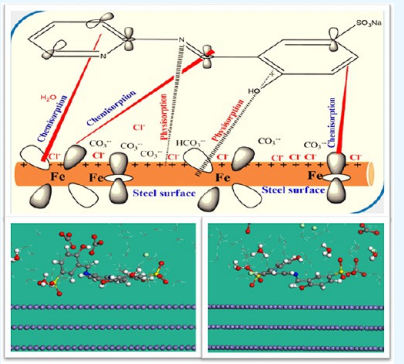

1. INTRODUCTION

It is well recognized that the alloy of carbon steel (CS), which displays a low carbon content of 0.18%, is readily obtainable, affordable, and used for a variety of implementations in the petroleum sectors.[1] Because of its strong mechanical characteristics as well as its economical nature, carbon steel, namely, C1018 steel, is frequently utilized in various industrial applications. Additionally, it is easily accessible, affordable, and strong enough to be used in a variety of acidic media in petrochemical operations like transportation, refining, and oil recovery. Consequently, the pipeline and oil sectors employ it extensively. These techniques are important because they improve oil recovery by removing industrialization-related salt deposits, undesirable scales, and mill scales.[2−9] Despite being the most widely used pipeline material in the petroleum industry, carbon steels are highly susceptible to corrosion in settings with carbon dioxide due to the practice of injecting CO_2 into oil wells to thin the oil's viscosity, improved oil recovery, and natural gas boost manufacture.[10,11] In the occurrence of dry carbon dioxide, carbon steel and alloys are not corroded by it. Diffusion of carbon dioxide corrosion would cause pipelines and structural elements in the production of petroleum to collapse, resulting in enormous financial losses, catastrophic accidents, pollution of water resources, and environmental degradation.[12,13] CO_2 dissolves in water to produce brine water, which then turns into carbonic acid, which is considered to be an extremely corrosive medium for carbon steel low alloy pipelines.[14−16] The most economical way to address this issue is by injecting corrosion inhibitors, particularly nitrogen-based organic compounds,[14] which can be used for reducing metal corrosion that contains hetero-atom functional groups, which can donate lone pairs of electrons.[17] Inhibitor compounds work in two steps, first transferring inhibitor species over a metal's interface and then having an obvious interaction with the functional groups of the steel by the adsorption phenomenon that protects the surface of the corrosive metal with lowering of its rate of the studied corrosion in hostile solutions.[18]

Schiff base and di-Schiff base aryl organic compounds are an active category of organic chemistry in many application areas, *e.g.*, in the field of biology[19] and as a ligandated backbone of

Received: January 27, 2023
Accepted: March 3, 2023
Published: March 14, 2023

transition metal complexes as highly effective catalysts in numerous organic transformations.[20] The low cost and facile synthesis of substituted Schiff base and di-Schiff base aryl organic compounds attract the attention of most chemists of organic and inorganic chemistry for designing more applicable derivatives with high potential in wide areas of applications. The most frequently used organic Schiff base inhibitors due to its higher inhibition than other amines,[21] which have heterocyclic organic molecules of highly attractive functional groups (*e.g.*, −C═C−, −N═N−, −CHO, −HC═N−, R−OH, etc.) conjugated double bonds and bigger electronegative atoms that such as (N, O, and S ....) have a predisposition to resist the rate of corrosive processes (CR) owing to the cathodic reaction, or anodic reaction, or both slowing down.[22]

Temperature variation is a highly helpful method for investigating and elucidating the adsorption mechanism of an inhibitor because it has a significant impact on the rate of metal corrosion. Although it is widely known that temperature has a highly complex influence, it does allow for the calculation of the thermodynamic adsorption and kinetic corrosion parameters, which aid in identifying the kind of adsorption of the investigated inhibitor.[23] In sweet conditions, depending on whether the solubility product of iron carbonate is surpassed, increasing the temperature can either raise or decrease the corrosion rate. The corrosion rate rises with rising temperature at low pH when the protective film does not form; however, at high pH, when the Fe^{2+} and CO_3^{2-} concentrations exceed the solubility limit, increasing the temperature will increase the precipitation rate and allow the development of a protective iron carbonate layer, and corrosion rate will decrease. Compared to surface films formed at low temperatures, those formed at high temperatures are continuous, compact, and more stable. Iron carbonate films have a protective quality that can get stronger at high temperatures.[24]

A comprehensive study on corrosion protection of di-Schiff base compounds in CO_2-satutared brine solution on C-steel has been attempted in the current work. Therefore, the main purpose of the current work is to explore the inhibition performance of Schiff base and di-Schiff base organic compounds as water-soluble inhibiting agents for sweet C-steel corrosion using EIS and PDP curves. The surface morphology of di-Schiff base molecules was detected by FE-SEM, and compositions of inhibitor surfaces were identified by EDS. The influence of solution temperature, inhibitor dose, and shaking speed was also investigated. An intensive study of DFT (density functional theory) with simulations of MD (molecular dynamics) was achieved using computational calculations to interpret the experimental results accomplished from the current work and to provide additional insight into the inhibitory action of the produced compounds on the C-steel interface.

2. EXPERIMENTAL SECTION

2.1. Methods and Devices. All the essential initial reagents and precursors were provided by Sigma-Aldrich, Merck, and BDH without any handling assigned. At room temperature, the main elements in the current Schiff base percentages were determined using a GMBH varioEI device (model V2.3). For the melting point determination, a Gallenkamp-Sanyo type device was used. Estimation of the nuclear magnetic resonance spectra (^{1}H and ^{13}C) in DMSO-d_6 for the three Schiff bases was accomplished using a Bruker FT-NMR multinuclear spectrometric device (model ARX400). The magnetic fields for carbon nuclei and hydrogen protons are 100.6 and 400.1 MHz, respectively. At ambient temperature, FTIR-spectroscopic scans of Schiff bases were examined through an Agilent Technology FTIR spectrophotometer (model Cary-630). A Jenway conductivity meter (model 4320) was applied to evaluate the conductivity of the three Schiff bases in two polar organic solvents. The epoxy-bodied conductivity cell, which has two shiny electrodes, was used for cell constant calibration at 25 ± 0.2 °C with a HAAKE ultrathermostat (model F3-k).

2.2. Synthesis of Schiff Base Compounds. *2.2.1. Sodium (E)-4-Hydroxy-3-((pyridin-2-ylimino)methyl)-benzenesulfonate (H1).* Sodium 2-hydroxybenzaldehyde-5-sulfonate (0.44 g, 2.0 mmol, in 25 mL of water) and 2-aminopyridine (0.08 g, 2.0 mmol, in 25 mL of methanol) were combined with constant stirring at room temperature. After 5 min of magnetic stirring, the mixture was heated at 75 °C for 2 h. TLC was used to follow the reaction progress. Then, the volatiles were detached under reduced pressure (with a vacuum), and the yellow color crude was crystallized from a mixture of H_2O/MeOH (1:1). The intended chemical was successfully synthesized as a yellow crystalline solid (88%), m.p. 121 °C, using a well-behaved crystallization of the Schiff base from the appropriate solvents.

^{1}H NMR in DMSO-d_6 (400 MHz): δ 6.51 (t, ^3J = 7.81 Hz, 1H), 6.74 (d, ^3J = 7.71 Hz, 1H), 6.91 (dd, ^3J = 8.1, 7.2 Hz, 1H), 7.22 (d, ^3J = 7.8 Hz, 1H), 7.63−7.75 (m, 2H), 7.93 (s, 1H), 10.25 (s, 1H), 13.23 ppm (s, 1H) (Figure S1, Supporting Information).

^{13}C NMR in DMSO-d_6 (100 MHz and dept-135): δ 111.05 (CH), 116.53 (CH), 124.45 (CH), 127.98 (CH), 129.94 (CH), 132.02 (CH), 137.89 (C_q), 152.55 (C_q), 156.77 (CH), 162.69 (C_q), 175.21 (C_q), 179.95 ppm (CH═N). The melting point is 231 °C (Figure S2, Supporting Information).

2.2.2. Sodium 3,3′-(1E,1′E)-(1,2-Phenylenebis(azan-1-yl-1-ylidene))bis(methan-1-yl-1-ylidene)bis(4-hydroxybenzenesulfonate) (H2). Sodium 2-hydroxybenzaldehyde-5-sulfonate (4.0 mmol, 0.88 g, in 50 mL of H_2O) was mixed with *o*-phenylenediamine (2.0 mmol, 0.21 g, in 25 mL of methanol) at 25 °C with constant stirring. The mixture was heated at 75 °C for 2 h after a short period of stirring. The reaction's development was observed using TLC. The volatiles were removed in a vacuum, and the yellow color crude was crystallized from a mixture of H_2O/MeOH (1:1). The required product was successfully extracted as a yellow crystalline solid (91%), m.p. 179 °C, from the di-Schiff base in a well-organized manner.

^{1}H NMR in DMSO-d_6 (400 MHz): δ 6.92 (t, ^3J = 6.9 Hz, 2H), 6.81 (d, ^3J = 7.5 Hz, 1H), 7.28 (d, ^3J = 7.7 Hz, 2 H), 7.623 (dd, ^4J = 1.8,^3J = 7.1 Hz, 2 H), 9.87 (s, 2 H), 12.41 ppm (s, 2 H, CH═N).

^{13}C NMR in DMSO-d_6 (100 MHz, dept-135): δ 110.92 (2 CH), 115.44 (2 CH), 124.44 (2 CH), 125.18 (2 CH), 129.77 (2 C_q), 133.69 (2 CH), 138.05 (2 C_q), 154.71 (2 C_q), 164.86 (2 C_q), 192.81 ppm (2 CH═N). The melting point is 272 °C.

2.2.3. Sodium 3,3′-(1E,1′E)-(4-Chloro-1,2-phenylene)bis-(azan-1-yl-1-ylidene)bis(methan-1-yl-1-ylidene)bis(4-hydroxybenzenesulfonate) (H3). Sodium salicylaldehyde-5-sulfonate (4.0 mmol, 0.88 g, in 50 mL of water) was mixed with 4-chloro-*o*-phenylenediamine (2.0 mmol, 0.28 g, in 25 mL of methanol) at 25 °C with continuous stirring. After a few minutes of stirring, the mixture was heated for 2 h at 75 °C. TLC was employed to keep track of the reaction's progress. The vacuum was used to extract the volatiles, and a solution of water and MeOH (1:1) was used to crystallize the yellow crude. The

https://doi.org/10.1021/acsomega.3c00561
ACS Omega 2023, 8, 11512−11535

Scheme 1. The Synthetic Path of Pyridyl-Schiff Base (H1) in Methanol

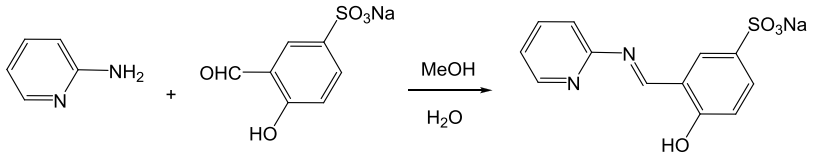

required product was produced in good yield as a yellow crystalline solid (87%), m.p. 190 °C, from the di-Schiff base, which crystallized well from the appropriate solvents.

^{1}H NMR in DMSO-d_6 (400 MHz): δ 6.94 (d, ^3J = 6.7 Hz, 1 H), 7.23 (d, ^3J = 6.2 Hz, 1 H), 7.72 (d, ^3J = 8.1 Hz, 1 H), 7.85 (d, ^3J = 7.9 Hz, 1 H), 7.96 (dd, ^4J = 2.0, ^3J = 7.8 Hz, 2 H), 9.37 (s, 1 H), 9.82 (s, 1 H), 10.35 (s, 1 H), 12.73 (s, 1 H, CH═N), 13.92 ppm (s, 1 H, CH═N).

^{13}C NMR DMSO-d_6 (100 MHz, dept-135): δ 113.72 (CH), 117.89 (CH), 122.14 (CH), 124.42 (C_q), 125.31 (CH), 127.68 (CH), 130.02 (C_q), 130.63 (CH), 133.65 (C_q), 139.87 (CH), 141.76 (CH), 143.35 (C_q), 145.16 (C_q), 155.11 (C_q), 158.06 (CH), 162.52 (C_q), 168.58 (C_q), 171.12 (C_q), 192.47 (CH═N), 197.36 ppm (CH═N). The melting point is 259 °C.

2.3. Sample Preparation for the Corrosion Inhibition Tests. As the working electrode (WE), C1018 carbon steel was used. It had a chemical structure (ASTM) (wt %) of 0.15% Cr, 0.25% C, 0.041% P, 0.89% Mn, 0.19% Si, and 0.035% S, and the remainder was Fe. The WE for the corrosion tests was a C-steel electrode put into an epoxy resin with a 0.713 cm^2 exposed area. The substrates were mechanically polished using a series of emery papers of increasing grades, starting with a rough one (800) and continuing on to the premium (1800) grade. The sample was only thoroughly cleaned with deionized H_2O followed by degreasing with acetone before being put inside the cell. A solution of 3.5% sodium chloride saturated with CO_2 was used as an aggressive medium. The required concentrations of inhibitor solutions (1×10^{-6}, 5×10^{-6}, 10^{-5}, 5×10^{-5}, 10^{-4}, 5×10^{-4}, 10^{-3} M) were prepared by dilution to 10^{-3} M, as a mother solution, of inhibitor, which was prepared by dissolving suitable weights in 3.5% NaCl followed by constantly bubbling with 99.999% pure CO_2 (1.0 h) to avoid corrosion initiated by O_2 at a pressure of 0.9 bar. Each study was performed using a brand-new solution and a variety of clean electrodes. Using the ultra-thermostat model Alpha RA 8, measurements were made for each electrode under investigation at 25 ± 0.5, 35 ± 0.5, 45 ± 0.5, and 55 ± 0.5 °C in the solutions under investigation. Between pH ∼4.0 and 4.4 of the solution preventing any progress in the mechanism of the corrosive system. All the experiments were accomplished at different shaking speeds from 200.0 to 500.0 rpm.

2.4. Corrosion Inhibition Measurements. Electrochemical methods are perfect for studying corrosion processes because corrosion is caused by electrochemical reactions.[25,26] Corrosion inhibition measurements comprising EIS as well as PDP curves were completed in a three-electrode cell assembly by means of a VersaSTAT4-400 potentiostat/galvanostat connected with a laptop. In this cell, the reference electrode, counter electrode, and working electrode are saturated calomel electrode (SCE), platinum sheet electrode, and C-steel, respectively. Because Schiff base compounds adsorbed to the C-steel alloy takes a certain amount of time, the C-steel samples were dipped in saturated sodium chloride (3.5%) of CO_2 having diverse doses of Schiff base compounds (H1, H2, and H3) for 50 min. After that, an almost stable state could be obtained for the open circuit potential (OCP). For EIS measurement, the NAB specimens were completed in a frequency variety of 100.0−10.0 MHz at the OCP with a square voltage of ±10 mV. The PDP plotting was given from E_{ocp} −250 mV to E_{ocp} +250 mV at a sweep rate of 0.2 mV s^{-1}. To establish the validity of the test, the electrochemical results were precisely reproduced three times.

2.5. Surface Morphologies and Description. The surface morphological structure of the metal surface before and after the addition of inhibitors was analyzed through SEM, *i.e.*, scanning electron microscope (JEOL), coupled with energy dispersive spectrometry (EDS). The C-steel specimens were immersed in the medium of corrosive processes without and with inhibitors for 48 h.

2.6. Theoretical Approaches. The energy minimization of the Schiff base derivative (H1, H2, and H3) compounds in aqueous solutions was studied using DFT calculations with the B3LYP-functional and DNP 4.4 basis set completed in the Dmol^3 module in the BIOVIA Materials Studio 2017 program.[27] From DFT calculation, the acquired outcomes including the highest occupied molecular orbital and lowest unoccupied molecular orbital (HOMO and LUMO, respectively) as well as the gap energy (ΔE), global softness (σ), electronegativity (χ), hardness (η), number of electrons transferred (ΔN), electrophilicity index (ω), dipole moment (μ), and $\Delta E_{\text{back-donation}}$ were inspected and calculated as follows:[1]

$$\chi = \frac{-E_{\text{HOMO}} - E_{\text{LUMO}}}{2} \tag{1}$$

$$\eta = \frac{1}{\sigma} = \frac{E_{\text{LUMO}} - E_{\text{HOMO}}}{2} \tag{2}$$

$$\omega = \frac{\chi^2}{2\eta} \tag{3}$$

$$\Delta N = \frac{\phi - \chi_{inh}}{2(\eta_{Fe} - \eta_{inh})} \tag{4}$$

$$\Delta E_{\text{back-donation}} = \frac{-\eta}{4} \tag{5}$$

where χ_{inh} indicates the electronegativity of inhibitor and φ is a function referring to the work of Fe (110). The chemical hardness of iron and the current inhibitor at 0 eV is represented by η_{Fe} and η_{inh}, respectively.

By using the adsorption finder module in the BIOVIA Materials Studio 2017 software, the correct adsorption arrangements of the Schiff base derivatives (H1, H2, and H3) on the Fe (110) interface were discovered for MC simulations.[28] First, for the optimization of the molecules of the adsorbate, the COMPASS force field was applied.[29] The adsorption of the tested inhibitors, chloride anions, hydronium anions, carbonate anions, and molecules of H_2O with the surface of iron (110) was then accomplished in a simulation box (37.24 × 37.24 × 59.81 Å).[30]

https://doi.org/10.1021/acsomega.3c00561
ACS Omega 2023, 8, 11512−11535

Scheme 2. The Synthetic Path of Di-Schiff Base (H2 and H3) in Methanol

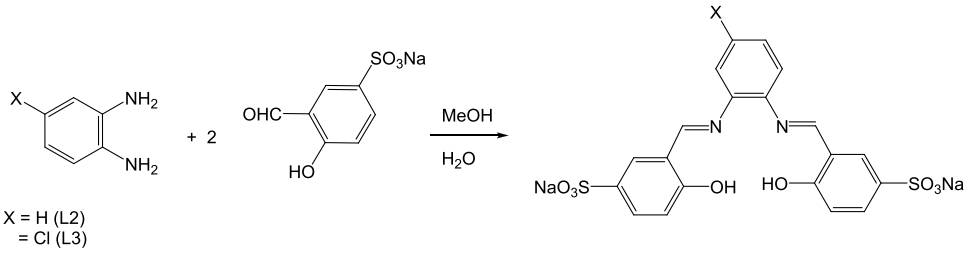

Table 1. The Percentage Analyses (CHN, %) of the Main Elements of H1, H2, and H3[a]

		CHN analyses, %			Λ_m, Ω^{-1} cm^2 mol^{-1}	
comp. (MW)	color	C	H	N	DMSO	DMF
H1 (300.27 g mol^{-1})	pale yellow	47.76 (48.00)	2.81 (3.02)	9.56 (9.33)	152	133
H2 (520.44 g mol^{-1})	yellow	46.92 (46.16)	2.79 (2.71)	5.04 (5.38)	201	226
H3 (554.88 g mol^{-1})	yellow	43.57 (43.29)	2.09 (2.36)	5.38 (5.05)	212	239

[a]Their color appearance and the conductivity measurements in DMSO and DMF (1.0 mmol dm^{-3}) at 25 °C.

3. RESULTS AND DISCUSSIONS

3.1. Preparation and Characterization. The facile condensation of equimolar amounts of 2-aminopyridine with sodium salicylaldehyde-5-sulfonate afforded the corresponding water-soluble Schiff base ligand (H1) with a good yield (Scheme 1).[31] The preparation of the di-Schiff base ligands (H2 and H3) required double the loaded amount of sodium salicylaldehyde-5-sulfonate to phenylenediamine or 4-chloro-*o*-phenylenediamine (Scheme 2), as reported previously.[32,33]

The main element analyses of CHN refer to the pure form of all Schiff base derivatives, which are listed in Table 1. The analyses of the percentages of the main elements are convenient with the proposed ones with less than 0.4% difference for H1, H2, and H3. Considerably, the high purity is deduced for the confirmation of their chemical structures (Schemes 1 and 2). The melting points for the three Schiff bases are 231, 272, and 259 °C, respectively, which are attributed to their high stability. The high melting points of the current Schiff bases could be interpreted by their salting nature, *i.e.*, the occurrence of the substituted ionic $-SO_3^-Na^+$ group.[31] The Schiff bases elucidate an illustrated stability area in various pH aqueous solutions from pH = 3.1 to 10.4 using universal buffer solutions.

In particular, H1, H2, and H3 are remarkably soluble in H_2O and organic solvents of high polar nature and strong coordinating characteristics, *e.g.*, *N*,*N*′-dimethylformamide (DMF) and dimethylsulfoxide (DMSO). Furthermore, the current Schiff bases are slightly soluble in polar organic solvents (*i.e.*, with high polarity) and in acetonitrile, ethanol, acetone, and methanol. The high solubility of the three Schiff bases could be a result of their strong conductivity behavior in the applicable solvents (DMF and DMSO) assigned to their polar nature.[34] The number of liberated ions in the solution could be estimated by the conductivity measurements. Hence, H1 gives two liberated ions per dissolved molecule: a cation of Na^+ and an anion of Schiff base sulfonate anion. On the other hand, H2 and H3 assign three free ions per molecule according to their conductivities: two Na^+ cations and one anion of the H2 and H3 with di-sulfonate anions.[34]

3.1.1. NMR Spectra. The deuterated solutions of the three Schiff bases in DMSO-d_6 at 25 °C and the NMR spectra for the ^{1}H- and ^{13}C-nuclei in H1, H2, and H3 are examined and recorded in the Experimental Section. The most distinguished functional protons of the Schiff base group are located at 13.22 and 12.41 ppm for H1 and H2, respectively. For H3, the two spectral signals for the two CH═N protons are also observed as a result of their unsymmetrical features (the substituted 5-chloro group). The two proton signals are located at 12.73 and 13.92 ppm as sharp signals. The other remarked proton could be recognized as the hydroxyl proton, which is positioned at 10.24 and 9.87 ppm for H1 and H2, whereas H3 shows two broad signals at 9.82 and 10.35 ppm for the hydroxyl protons. The other spectral signals for H1, H2, and H3 belong to the aryl rings.

For the absorption spectra of carbon nuclei for H1, H2, and H3, the most remarkable downfield shifted signals belonged to the Schiff base group, which are displayed at 179.95 and 192.81 ppm for H1 and H2, respectively, and two signals at 197.36 and 192.47 ppm for H3. The symmetric C−O nuclei are observed at 162.70 and 164.86 ppm for H1 and H2, but the asymmetric C−O nuclei in H3 are positioned at 168.58 and 171.12 ppm. The other spectral signals are assigned to the aromatic carbons.

3.1.2. IR Spectra. The samples of H1, H2, and H3 are measured for infrared spectroscopy, and the considered spectral bands are given and recorded in Table 2. The resonating bands of OH bond in H1, H2, and H3 are located at 3166, 3291, and 3302 cm^{-1} as broad bands.[31] The azomethine band (CH═N) is observed with a sharp band shape of vibration at 1665 and 1574 cm^{-1} for H1 and H2, whereas it is found as two bands at 1572 and 1519 cm^{-1} for the asymmetric CH═N bonds in H3. The

Table 2. Assigned IR Spectral Results ($\bar{\nu}$, cm^{-1}) for H1, H2, and H3

	comp.		
group	H1	H2	H3
O—H$_{(phenolic)}$	3166	3291	3302
C—H$_{ar}$	3095	3016	3035
C—O$_{(phenolic)}$	1480	1373	1393
C═N$_{(azomethine)}$	1665	1574	1572, 1519
C—N$_{(azomethine)}$	1101	1099	1052, 1012
C═N$_{(py)}$	1588		
C—N$_{(py)}$	1026		
S═O	1429	1446	1447
S—O$^-$	1165	1149	1159

https://doi.org/10.1021/acsomega.3c00561
ACS Omega 2023, 8, 11512−11535

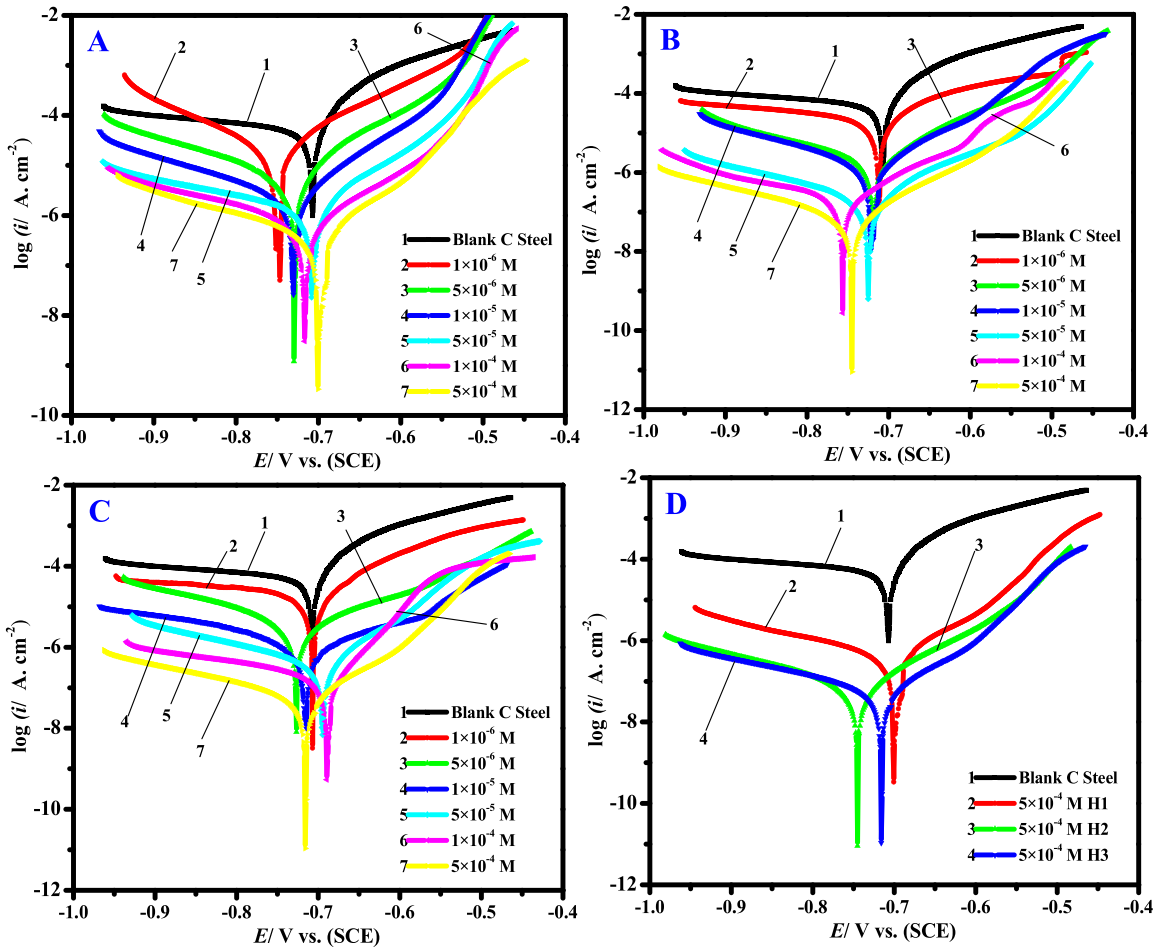

Figure 1. PDP diagrams of C-steel corrosion in the blank sweet oilfield environment and with addition of varied doses of prepared Schiff base compounds (A) H1, (B) H2, and (C) H3 and (d) in the occurrence of the optimum dose of 0.5 mM of (line 1) H1, (line 2) H2, and (line 3) H3 at 55 °C.

Table 3. PDP Restrictions of C-Steel Corrosion in the Blank Sweet Oilfield Environment and with Addition of Different Concentrations of the Synthesized Schiff Base Inhibitors at 55 °C

inhibitors code	$C_{inh.}$ (mol/L)	i_{cor} (μA cm^{-2} ± SD)	$-E_{cor}$ (mV (SCE))	β_a (mV dec^{-1})	$-\beta_c$ (mV dec^{-1})	θ	η_t (%)
blank	0.0	743.6 ± 32.3	705 ± 33	100.2	198.8		
H1	1.0×10^{-6}	558.4 ± 23.2	745 ± 43	107.3	182.7	0.249	24.9
	5.0×10^{-6}	501.1 ± 31.4	727 ± 41	106.2	195.2	0.326	32.6
	1.0×10^{-5}	368.8 ± 23.4	729 ± 29	102.6	199.1	0.504	50.4
	5.0×10^{-5}	250.5 ± 17.4	708 ± 52	105.3	198.2	0.663	66.3
	1.0×10^{-4}	120.4 ± 9.3	716 ± 36	113.2	205.1	0.838	83.8
	5.0×10^{-4}	55.7 ± 3.7	702 ± 31	98.4	204.9	0.925	92.5
H2	1.0×10^{-6}	533.1 ± 32.7	712 ± 26	101.8	198.8	0.283	28.3
	5.0×10^{-6}	449.1 ± 31.3	719 ± 19	88.9	203.9	0.396	39.6
	1.0×10^{-5}	315.2 ± 22.5	721 ± 47	97.5	197.1	0.576	57.6
	5.0×10^{-5}	197.8 ± 12.1	727 ± 39	112.1	200.3	0.734	73.4
	1.0×10^{-4}	109.3 ± 7.8	757 ± 51	98.7	198.4	0.853	85.3
	5.0×10^{-4}	31.9 ± 2.2	742 ± 28	89.7	193.5	0.957	95.7
H3	1.0×10^{-6}	506.4 ± 42.4	705 ± 23	108.5	189.3	0.319	31.9
	5.0×10^{-6}	418.6 ± 27.8	725 ± 34	85.9	193.3	0.437	43.7
	1.0×10^{-5}	258.1 ± 14.5	713 ± 35	99.2	188.2	0.653	65.3
	5.0×10^{-5}	167.3 ± 11.2	695 ± 44	106.2	190.6	0.775	77.5
	1.0×10^{-4}	78.1 ± 5.3	688 ± 17	102.8	189.4	0.895	89.5
	5.0×10^{-4}	10.4 ± 1.1	710 ± 22	88.7	193.5	0.986	98.6

band of the C═N bond of the pyridyl ring in H1 is positioned at 1588 cm^{-1} (Table 2). The sulfonate group shows two bands for the two bonds of (S═O double bond and S−O single bond), which are assigned at 1429 and 1165 cm^{-1} for H1, 1446 and

https://doi.org/10.1021/acsomega.3c00561
ACS Omega 2023, 8, 11512−11535

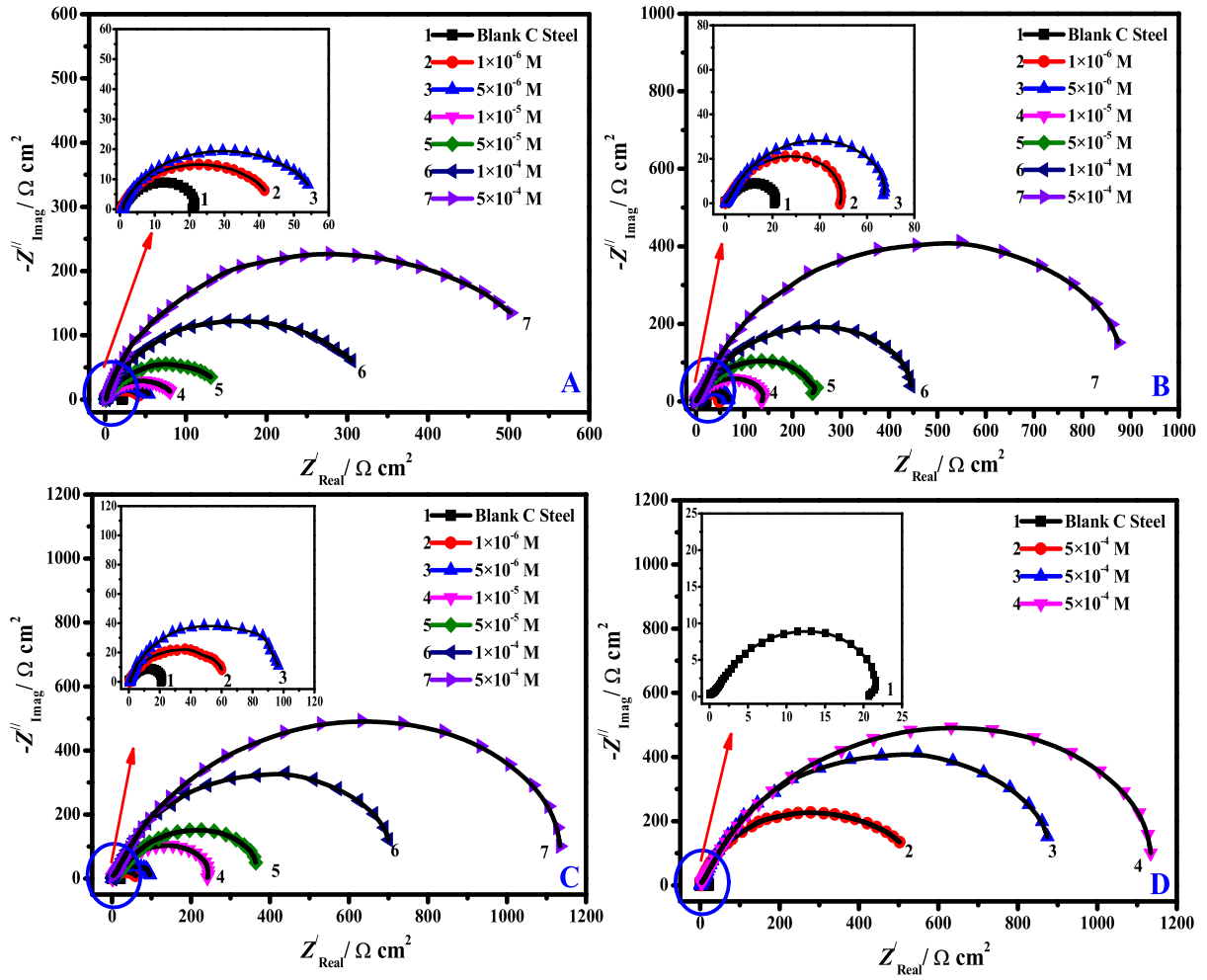

Figure 2. Nyquist diagrams of C-steel corrosion in the blank sweet oilfield environment and with addition of different concentrations of prepared Schiff base compounds (A) H1, (B) H2, and (C) H3 and (D) in the occurrence of the optimum dose of 0.5 mM of (line 2) H1, (line 3) H2, and (line 4) H3 at 55 °C.

1149 cm^{-1} for H2, and 1447 and 1159 cm^{-1} for H3, respectively.[34]

3.2. Corrosion Protection Performance. *3.2.1. Inhibitor Dose Effect. 3.2.1.1. PDP Studies.* The Tafel plot is an approach for calculating the kinetics and rate of the corrosion pathways by analyzing the experience polarization graphs. Figure 1 displays the PDP profiles for the C-steel corrosion in the blank sweet oilfield environment and with addition of various doses of prepared Schiff base compounds (A) H1, (B) H2, and (C) H3 and (D) in the existence of an optimal concentrated solution (*i.e.*, 0.5 mM) of H1, H2, and H3 at 55 °C. Tafel's performance can be seen in both the anodic and cathodic portions of the polarization curves. It is obavious that the occurrence of the Schiff base H1, H2, and H3 compounds results in a significant reduction in the corrosion rate, in which both cathodic and anodic parts of the Tafel graphs are conjointly modified to slight current values at completely investigated concentrations. The similar cathodic Tafel shapes in Figure 1 display that the hydrogen progression was activation-controlled and that the presence of the H1, H2, and H3 compounds had no effect on the cathodic reaction of H_2 progress.[35] The successful adsorping attractions of the inhibiting Schiff base compounds to the steel interface have taken place, causing the blocking of the active centers of the corrosive progression on the steel interface. As a result, the surface is submerged and constrained by hydrogen ion deteriorations, but the mechanistic pathway of such process breaks is not influenced.

The parameter values of Tafel, for example, corrosion current density (i_{cor}), corrosion potential (E_{cor}), and Tafel anodic (β_a) and cathodic (β_c) slopes, were attained by the well-explored extrapolation Tafel plot. Hence, the results are documented for various inhibitor concentrations in Table 3, and i_{cor} is computed from the anodic and cathodic branched extrapolation to the E_{cor}. The reliable protection ability (η_t/%) with the covered part of the steel surface (θ) was determined using the following equation:[36]

$$\eta_t/\% = \left(\frac{i_{cor,0} - i_{cor,i}}{i_{cor,0}}\right) \times 100 = \theta \times 100 \quad (6)$$

where $i_{cor,0}$ and $i_{cor,i}$ denote, respectively, the blank (inhibitor-free) and inhibited i_{cor}. The examination of Table 3 discloses that the i_{cor} in the presence of 5.0×10^{-4} M of Schiff base H1, H2, and H3 compounds is impartially smaller (55.7 $\mu A/cm^2$ for H1, 31.9 $\mu A/cm^2$ for H2, and 10.4 $\mu A/cm^2$ for H3) as compared to that of the uninhibited corrosive solution (743.6 $\mu A/cm^2$). When the Schiff base H1, H2, and H3 compounds were inserted into the harsh atmosphere, the protection power increased, and the extreme values of η_t/% were 92.5, 95.7, and 98.5% at the optimal concentration (5.0×10^{-4} M) for H1, H2, and H3, respectively,

https://doi.org/10.1021/acsomega.3c00561
ACS Omega 2023, 8, 11512−11535

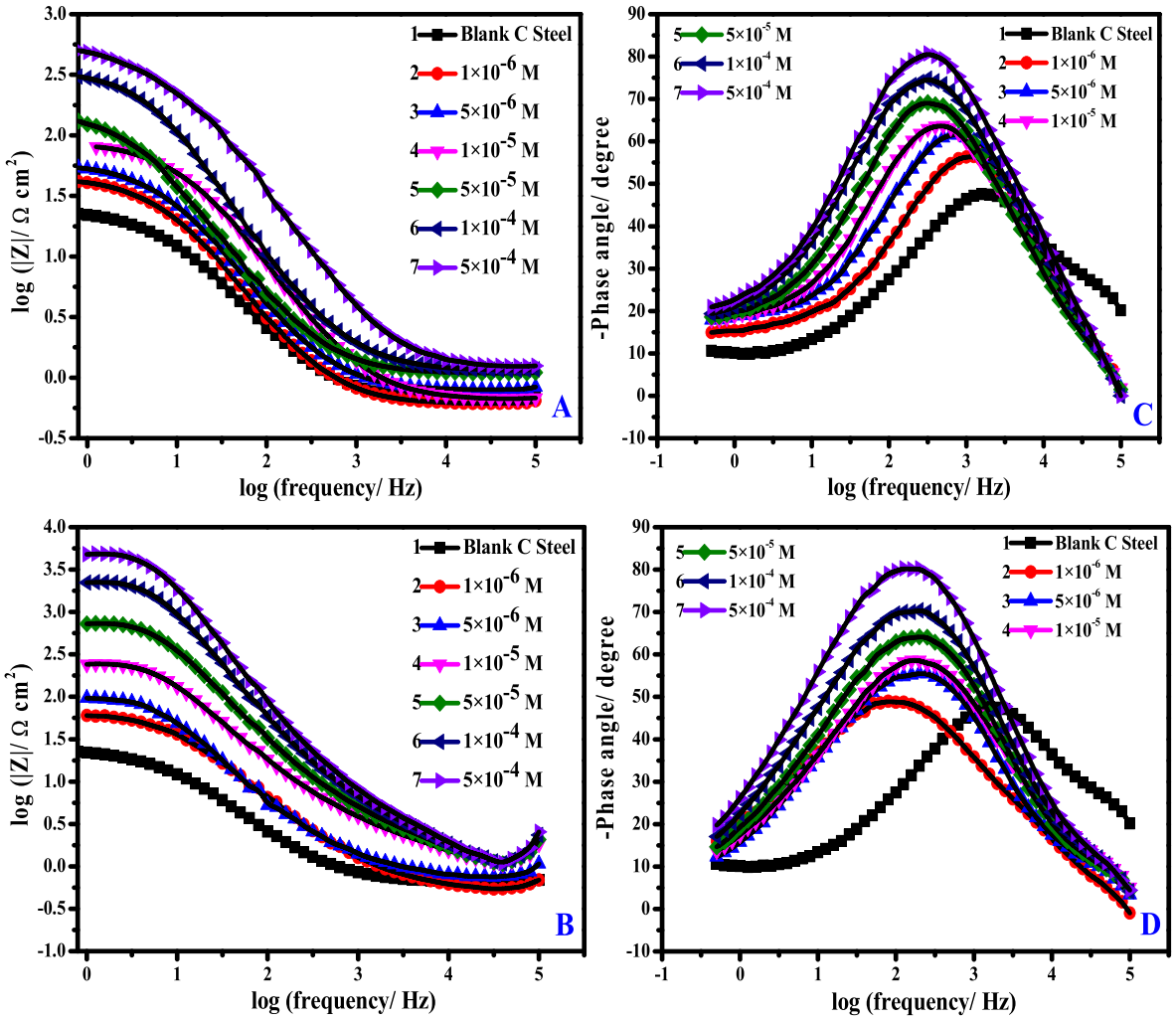

Figure 3. Bode (A, B) and Bode phase (C, D) of C-steel corrosion in the blank sweet oilfield environment and with addition of different doses of prepared Schiff base compounds (A, C) H1, and (B, D) H3 at 55 °C.

representing that a larger quantity of the protected surface is reached in the harsh atmosphere with the supreme dose of Schiff base H1, H2, and H3 compounds,[37] which is supported by an increase in surface coverage (cf. Table 3). Table 3 shows that the modifications of both β_c and β_a, *i.e.*, cathodic anodic values, respectively, are not obvious according to the outcomes from the blank medium. These indicate that all current Schiff base H1, H2, and H3 compounds could be successfully adsorbed on the metal surface to minimize the number of efficient sites at the metal interface rather than by altering the anodic and cathodic mechanistic pathway to impede such corrosive process.[38] According to the Tafel plots, the presence of Schiff base H1, H2, and H3 compounds causes a minimizing of the anodic/cathodic current density but not a substantial change in E_{cor} values (the maximum change in E_{cor} is 40 mV). According to literature studies,[39,40] an anodic or cathodic type of inhibiting reagent can be identified if the displacement in E_{cor} is greater than 85 mV in comparison to E_{cor} of the uninhibited medium. As a result, at 55 °C, all of the investigated Schiff base H1, H2, and H3 compounds function as mixed-type additives.

For these Schiff base H1, H2, and H3 compounds, the inhibitive proficiency orders are H3 > H2 > H1. This is the explanation for the adhesion of Schiff base molecular species to the steel surfaces and obstructing the sites of corrosion to protect it from corrosion degradation.

3.2.1.2. EIS Examinations. For further reorganization of the corrosive mitigation influence of the Schiff base H1, H2, and H3 compounds, EIS works of various uninhibitive and inhibitive media were performed. The prepared Schiff base H1, H2, and H3 compounds were used for inhibition examinations of the C-steel in a sweet oilfield environment using EIS at E_{OCP}. The Nyquist (Z_{real} vs Z_{imag}) and Bode plots of the steel alloy surfaces' kinetics of corrosion mitigation were perfectly designed by the EIS investigations. In Figures 2 and 3, respectively, the impedance results for the present investigation are shown as Nyquist and Bode plots.

As depicted in the plotting of Figure 2, Nyquist plots are revealed as a single semicircle, demonstrating how charge transfer at the interface of the metal/solution and the capacitance of the double layer (C_{dl}) are responsible for C-steel deterioration in the investigated aggressive solution lacking and with Schiff base H1, H2, and H3 compounds.[41] The Nyquist diagram displays a comparable behavior at entirely experienced doses, demonstrating that the addition of Schiff base H1, H2, and H3 additives to the harch solution has no effect on the mode of the corrosive action.[42] Futhermore, the semicircle widths get wider when the concentration of a Schiff base additive in the

https://doi.org/10.1021/acsomega.3c00561
ACS Omega 2023, 8, 11512−11535

experimental medium upsurges. The dispersal impact in frequency is an indication that the middles of Nyquist depressed circles were below the actual axis.[43] This behavior may be produced by the metal's coarse interface; the surface's possibility for heterogeneity, predominantly at grain boundaries; and the Schiff base H1, H2, and H3 additives' desorption/adsorption approach at the surface of the studied steel.[44] The value of α, which signifies the steel surface roughness, was computed from the linear portion slope log(f) vs log|Z| diagrams (Figure 3A,B). Hypothetically, for an impeccable capacitor, the α value would be −1. In the CO_2-saturated brine (blank and inhibited systems), it was found that the α parameter of the C-steel was less than unity. Such behavior was ascribed to the corrosive process of steel in the aggressive medium that initiated the steel surface to be coarse and, accordingly, the metal surface to become heterogeneous. Furthermore, the magnitudes of phase angle at middle frequency are −48.1, −80.3, and −81.5° for the blank and inhibitor containing system with 5.0×10^{-4} M of H1 and H3, respectively. The enhancement of the phase angle in the presence of H1 and H3 molecules proposes that the capacitive routine of the surface of the metal/solution is being characterized by the adsorption of Schiff base compounds.[45] The protective performance occurred because more H1 and H3 additives were adsorbed at the metal/electrolyte interface, developing an inhibitor−Fe complexing behavior, which was capable to protect the metal surface from deterioration and, as a consequence, gave increase to a small corrosion rate. This is depicted in Figures 3C,D. According to the Nyquist and Bode phase modules, such can be seen that there is one of both semicircle and peak, respectively. Therefore, these outcomes demonstrated an observed distinct time constant in the electrochemical route, which was associated to the double electrical film created at the interface of C-steel/electrolyte. The comparison of fitted and investigational findings of C-steel corrosion in the blank sweet oilfield environment (A) and after mixing with 5×10^{-4} mol/L H3 is illustrated in Figure 4. Utilizing the equivalent circuit example assigned in Figure 4A,B inset, the abbreviation EIS parameters were evaluated. The ideal equivalent circuit (EEC) (Figure 4 inset) was utilized to obtain the impedance characteristics to mathematically interpret the electrochemical performance. The EEC illustrated in Figure 4A inset was utilized to normalize the results of the inhibitor-free (blank) system, whereas Figure 4B inset provides an example of the occurrence of 0.5 mmol/L H3 compound. Table 4 contains a record of the EEC's appropriate accuracy (χ^2). The quite low value of the χ^2 in Table 4 indicates that our fitting process is valid.[46]

This EEC prototype that satisfies the EIS indices comprises the resistance of the studied electrolyte (R_{elec}), the constant phase element (CPE), and the magnitude of the resistance of the polarization (R_p) [R_p = R_f (the layer resistance) + R_{ct} (the resistance of the charge transfer through the electrolyte)]. This could be in sequence to the parallel of the adsorption layer capacitance (C_{ads}) and the adsorption resistance of film (R_{ads}) in the case of inhibited medium. The heterogeneous phase and roughness of the C-steel precursor caused a dispersion influence in such stage; hence, CPE was used instead of pure capacitance to counteract it. The impedance magnitude of CPE (Z_{CPE}) is precisely identified by the following equation:[1]

$$Z_{CPE} = \frac{1}{(j\omega)^n \times Y_0} \tag{7}$$

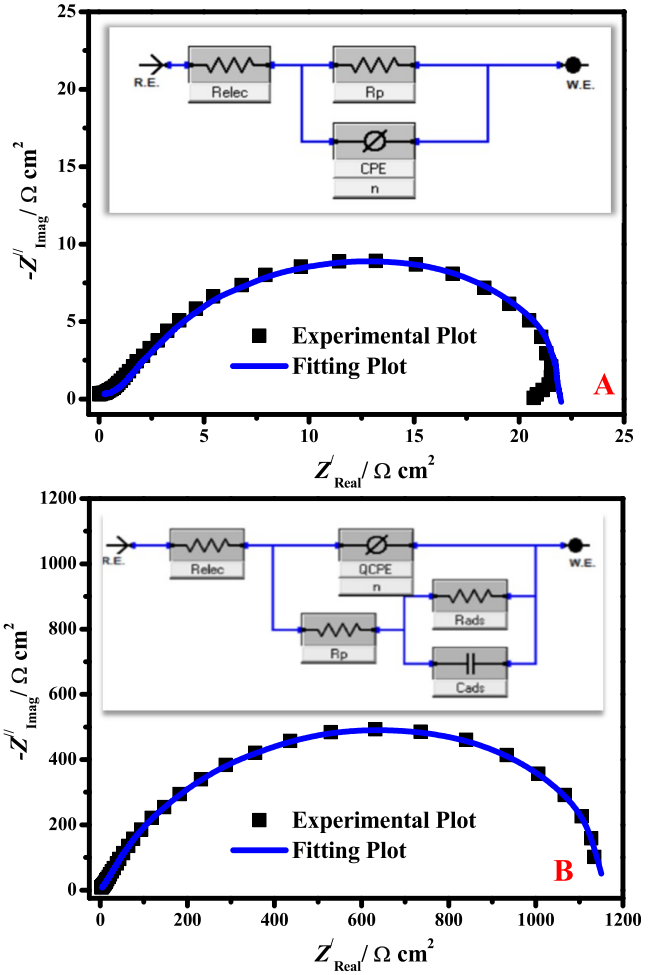

Figure 4. Comparison of fitted and investigational findings of C-steel corrosion in the blank sweet oilfield environment (A) and with addition of 0.5 mmol/L H3 (B).; inset the EEC of blank (A) and inhibited systems (B).

where ω symbolizes the angular frequency, Y_o denotes the CPE's modulus, j symbolizes the imaginary number, and n stands for a phase shift. CPE designates a pure resistor if n = 0, an inductor if n = −1, and a perfect capacitor if n = 1. Consistent with the results in Table 4, we could determine that the insertion of the Schiff base H1, H2, and H3 compounds to the studied harsh solution becomes adsorbed on the C-steel interface by replacing the molecules of water. Additionally, we observed that the steel substrate was much more homogeneous in the protected systems, as indicated by the marginally higher n value for the protected organizations in comparison to the values in the blank system, which measures the degree of heterogeneity. This is a result of the Schiff base H1, H2, and H3 compounds uniformly adhering to the steel substrate.[47] The inhibition ability (η_E/%) and C_{dl} values were computed as follows:[48]

$$C_{dl} = [(R_{ct})^{1-n} \times Y_0]^{1/n} \tag{8}$$

$$\eta_E/\% = \left(\frac{R_{P,i} - R_{P,u}}{R_{P,i}}\right) \times 100 \tag{9}$$

where $R_{P,u}$ and $R_{P,i}$ refer to the particular resistance of polarization for C-steel in the blank and protected systems, respectively. Table 4 displays the R_p values, showing an increase

https://doi.org/10.1021/acsomega.3c00561
ACS Omega 2023, 8, 11512−11535

Table 4. EIS Parameters of C-Steel Corrosion in the Blank Sweet Oilfield Environment and with Addition of Various Doses of Prepared Schiff Base Compounds at 55 °C

					Q_{CPE}				
inhibitor codes	$C_{inh.}$ (mol/L)	R_s (Ω cm^2)	R_P (Ω cm^2 ± SD)	C_{dl} (F cm^{-2} × 10^{-6})	Y_0 ($\mu\Omega^{-1}$ s^n cm^{-2})	n	χ^2 (×10^{-4})	θ	η_E (%)
blank	0.0	0.91	21.8 ± 1.3	436.65	55.43	0.725	4.95		
H1	1.0 × 10^{-6}	1.16	45.3 ± 3.2	175.23	34.31	0.855	4.08	0.518	51.8
	5.0 × 10^{-6}	1.83	62.2 ± 5.6	141.61	24.76	0.877	4.09	0.649	64.9
	1.0 × 10^{-5}	2.08	94.4 ± 7.3	79.15	18.12	0.865	4.91	0.769	76.9
	5.0 × 10^{-5}	2.58	173.2 ± 13.6	41.38	10.38	0.888	4.28	0.874	87.4
	1.0 × 10^{-4}	2.83	378.8 ± 21.8	34.07	7.22	0.843	4.99	0.942	94.2
	5.0 × 10^{-4}	3.08	634.2 ± 32.9	30.92	2.92	0.865	4.93	0.965	96.5
H2	1.0 × 10^{-6}	1.08	49.8 ± 2.8	139.15	26.60	0.809	4.86	0.562	56.2
	5.0 × 10^{-6}	1.41	72.1 ± 5.6	114.44	19.08	0.826	3.61	0.697	69.7
	1.0 × 10^{-5}	1.91	145.7 ± 9.8	72.67	14.08	0.858	4.66	0.851	85.1
	5.0 × 10^{-5}	2.91	292.1 ± 16.9	22.92	8.24	0.843	4.86	0.925	92.5
	1.0 × 10^{-4}	3.22	459.4 ± 27.2	18.23	5.79	0.869	4.60	0.952	95.2
	5.0 × 10^{-4}	4.91	950.2 ± 46.5	12.34	2.38	0.893	4.89	0.977	97.7
H3	1.0 × 10^{-6}	1.18	67.6 ± 5.1	89.20	18.42	0.808	4.94	0.677	67.7
	5.0 × 10^{-6}	1.54	119.1 ± 8.6	73.64	13.21	0.818	3.66	0.816	81.6
	1.0 × 10^{-5}	2.09	280.6 ± 15.5	46.15	9.25	0.844	4.74	0.922	92.2
	5.0 × 10^{-5}	3.18	439.1 ± 28.3	14.68	5.78	0.835	4.94	0.950	95.0
	1.0 × 10^{-4}	3.27	782.6 ± 41.7	11.69	3.83	0.867	4.62	0.972	97.2
	5.0 × 10^{-4}	5.36	1176.2 ± 67.9	7.96	1.42	0.884	4.47	0.981	98.1

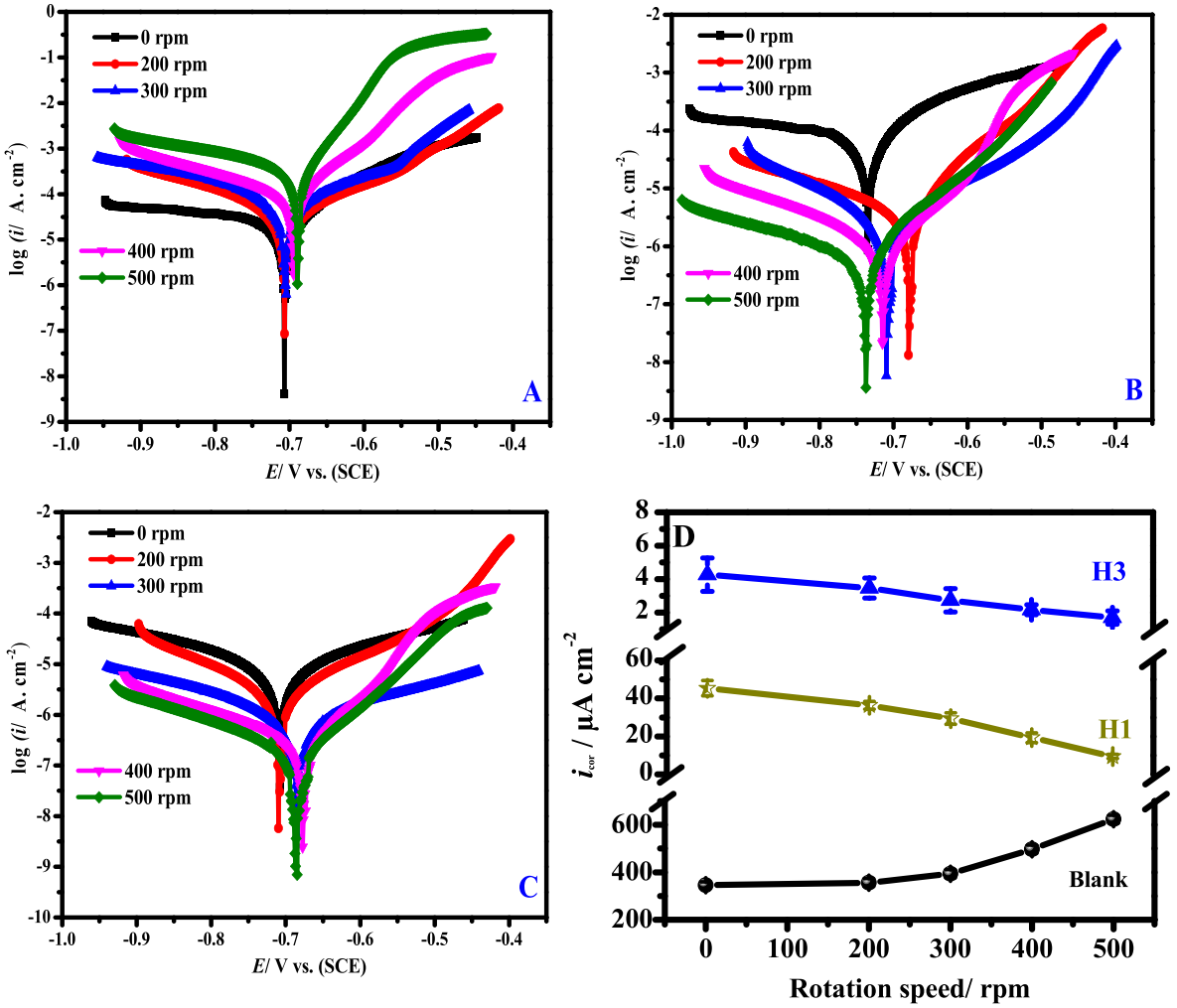

Figure 5. PDP plots for C-steel in the blank sweet oilfield environment (A) and with addition of 0.5 mmol/L H1 (B) and 0.5 mmol/L H3 (C) at diverse rotation speeds. Variance of i_{cor} with rotation speed (rpm) in the blank and inhibited medium (D).

https://doi.org/10.1021/acsomega.3c00561
ACS Omega 2023, 8, 11512−11535

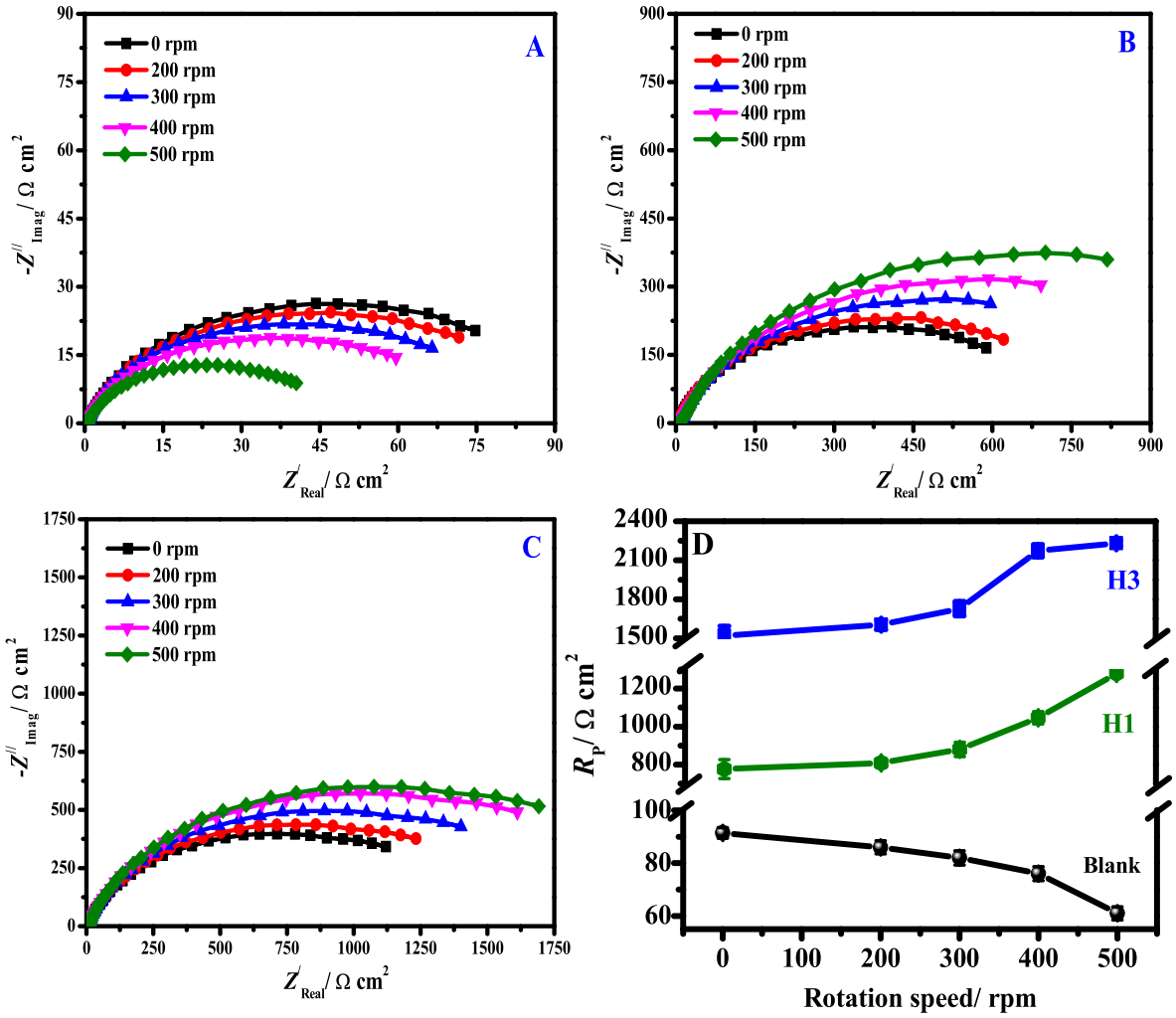

Figure 6. Nyquist diagrams for C-steel in the blank sweet oilfield environment (A) and with addition of 0.5 mmol/L H1 (B) and 0.5 mmol/L H3(C) at diverse rotation speeds. Variance of R_p with rotation speed (rpm) in the blank and inhibited medium (D).

in values through an upsurge within the inhibiting dose. These values are greater than those of the blank medium. The R_p value improved from 21.8 ± 1.3 to 634.2 ± 32.9, 950.2 ± 46.5, and 1176.2 ± 67.9 Ω cm^2 when the dose of Schiff base H1, H2, and H3 compounds reached 0.5 mmol L^{-1}, respectively. Consequently, the inhibition ability of 96.5, 97.7, and 98.1% was proficient, demonstrating the promising corrosion mitigation by Schiff base H1, H2, and H3 compounds for C-steel in saturated NaCl (3.5%) soution with CO_2. Because more of the surface is coated by the inhibiting Schiff base additives, which are accountable for the diminished steel corrosion, the values of R_p and η_E/% increase with an upsurge in inhibitor dose.[49] But compared to the blank medium, the C_{dl} values diminished with a rise in Schiff base, which suggests that additive molecules may have adhered to the metal surfaces and caused the preadsorbed H_2O molecules to fragment, decreasing the electrical ability of the electrode surface. According to Helmholtz's illustration, this tendency of C_{dl} is associated with an upsurge in the defensive film's thickness (L) or a decline in the comparative dielectric constant (c) as revealed by eq 10:[50]

$$C_{dl} = \frac{\varepsilon_c \varepsilon_0}{L} \tag{10}$$

Accurately, the H1, H2, and H3 compounds' adsorption process on the steel surface resulted in an upsurge in L and decline in ε. Therefore, C_{dl} speciously lessened for C-steel in the inhibited system. These outcomes display once more that the protection route for H1, H2, and H3 chemicals proceeds through the adsorption process onto the metal substrate and are in well covenant with those of PDP studies.

3.2.2. Influence of Stirring Conditions. In actual industrial organizations, it is necessary to examine the impacts of the flow circumstances of the aggressive media containing inhibiting compounds. In prior investigations,[49] magnetic stirring was applied to demonstrate flow circumstances. PDP studies for C-steel in the blank sweet oilfield environment (A) and with addition of 0.5 mmol/L H1 (B) and 0.5 mmol/L H3(C) at diverse rotation speeds are exhibited in Figure 5A−C. The variation of i_{cor} with rotation speed (rpm) in the uninhibited and inhibitor containing system is depicted in Figure 5D. The value of i_{cor} rises for the blank system (Figure 5A) as the rotational speed increases, reaching its maximum value at 500 rpm.

There was little change in the PDP plotting significant for the inhibited system at the various rotation speeds, as observed in Figure 5B,C. Consequently, at static conditions, E_{cor} values of −0.733 and −0.707 mV vs SCE and i_{cor} values of approximately 45.41 and 4.26 μA/cm^2 in the existence of 5 × 10^{-4} mol/L H1 and H3, respectively, were accomplished. The i_{cor} value diminished slightly, reaching its lowest value at 500 rpm, whereas the E_{cor} value grew in efficiency and remained more or

https://doi.org/10.1021/acsomega.3c00561
ACS Omega 2023, 8, 11512−11535

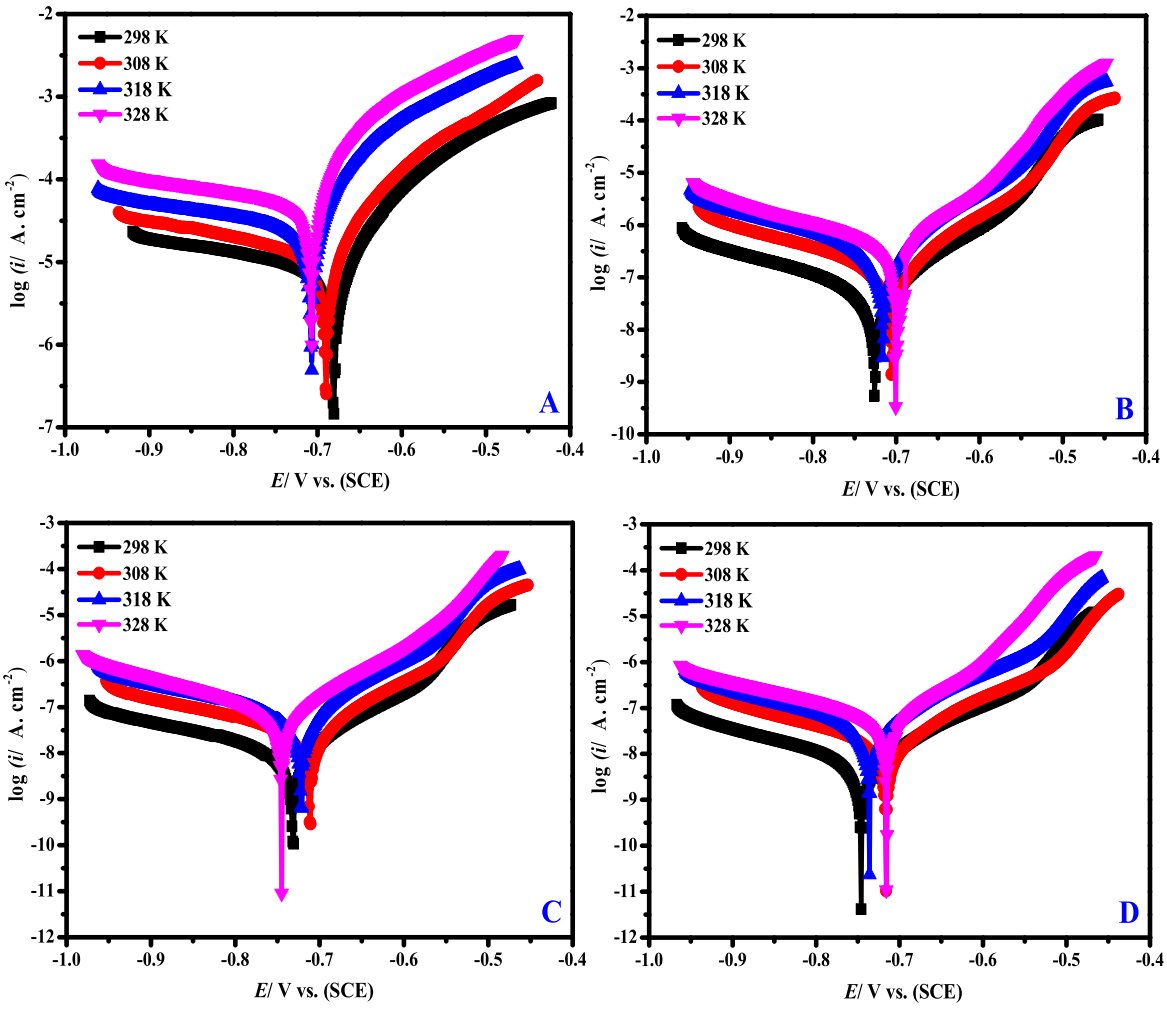

Figure 7. PDP plots for C-steel in the blank sweet oilfield environment (A) and with addition of 0.5 mmol/L H1 (B), 0.5 mmol/L H2 (C), and 0.5 mmol/L H3 (D) at diverse temperatures.

less consistent around −0.737 mV for H1 and −0.683 mV for H3 (Figure 5B,C).

Comparing the results at the same rotation speed, it was realized that when the system was in a stagnant state and additives were added to the corrosive medium, the values of i_{cor} increased (Figure 5D); nevertheless, for the magnetic stirring of the solution, these i_{cor} values obtained decreased because of the existence of H1 and H3 Schiff bases in relation to the rotation speed value. This effect may be explained by the flow surge in the mass transition of inhibiting species (molecules) that results in further inhibiting action presence at the metal surface. This influence might intensify the inhibitory mode.[50]

The EIS approach is used to examine the impact of rotation speed at various rpm values (from 0 to 500 rpm). Figure 6 displays Nyquist graphs for C-steel in the blank sweet oilfield environment (A) and with addition of 0.5 mmol/L H1 (B) and 0.5 mmol/L H3 (C) at diverse rotation speeds. Figure 6D shows how R_p values vary with rotational speed (in rpm) in several corrosive systems. The increase in stirring rate (rpm) in the inhibitor-free medium (blank) exceeds the increase in corrosion rate, resulting in a decrease in R_p. When H1 and H3 compounds are present, the Nyquist semicircle's diameter grows along with a rise in rotational speed (rpm), demonstrating a decline in the corrosion rate. This is explained by the compact nature and complete coverage of the protective sheet H1 and H3 compounds adsorbed at the metal/electrolyte interface. Apparently, the stirring flow enhances not only the association of the chloride and dissolved oxygen but moreover the obvious movement of the H1 and H3 compounds to the steel substrate, resulting in a protective coating that is less permeable and has good surface coverage.

3.2.3. Temperature Effect on the Corrosion Mitigation Route and the Thermodynamic Activation Restrictions. In a blank and inhibited experiment system, the influence of temperature on steel dissolution was examined. PDP was conducted at various temperatures (298.0−328.0 K) for the investigated electrode in a sweet oilfield environment lacking and with specific doses of the current Schiff base H1, H2, and H3 inhibitors to learn more about the adsorption type at higher temperatures and efficiency of the prepared Schiff base as corrosive inhibiting agents. The analysis of these data may provide a suggestion for the way of adsorption (chemisorption or physisorption). As the temperature rises, chemisorption is strengthened, but at lower temperatures, physical adsorption predominates.[8]

PDP curves for C-steel in the blank sweet oilfield environment (A) and with addition of 0.5 mmol L^{-1} H1 (B), 0.5 mmol L^{-1} H2 (C), and 0.5 mmol L^{-1} H3 (D) at diverse temperatures are represented in Figure 7A−D. According to the information in Figure 7, there is a significant cathodic and anodic branch

https://doi.org/10.1021/acsomega.3c00561
ACS Omega 2023, 8, 11512−11535

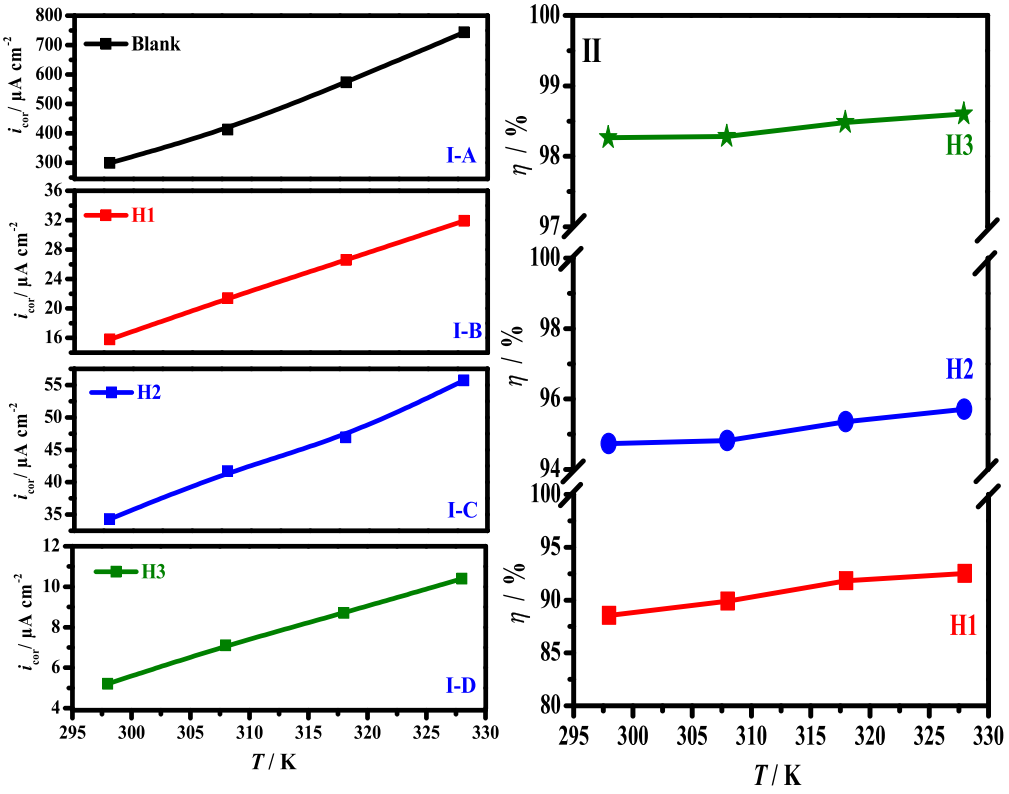

Figure 8. Change of corrosion current density (i_{cor}) (I) and the inhibition capability (η/%) (II) with temperature (K) in varied corrosion solutions.

precipitation that corresponds with an increase in the reaction temperature. The Tafel slopes (cathodic β_c and anodic β_a) of the polarization diagrams are also not noticeably altered as temperature increases. In covenant with the electrode acceleration deterioration at enhanced medium temperatures, the values of E_{cor} are primarily changed in a more positive direction with increasing temperature.

Figure 8I,II displays the variant of corrosive current density (i_{cor}) (I) and the inhibitive capability (η/%) (II) with the absolute solution temperature (K) in varied corrosion media. In Figure 8I, it was possible to see that for the metal in an uninhibited solution, i_{cor} increases with temperature (inhibitor-free). Based on the fact that increasing the solution temperature speeds up all other corrosion routes, including electrochemical and chemical reactions and the diffusion of reactive species to the electrode surface, this phenomenon can be explained.[8] The i_{cor} for the inhibited systems is consistently lower than that for the blank systems. These findings indicate that the examined temperature range is suitable for the H1, H2, and H3 Schiff base inhibitors. Figure 8II shows the effect of varied temperatures of investigated Schiff base H1, H2, and H3 compounds on the inhibition capability of C-steel in three sweet oilfield environments. This diagram shows that when the solution temperature rises, the protective capacity increases. Chemical adsorption is the distinguishing factor in this performance. This is because raising the reaction temperature strengthens the attraction between inhibitor species and the metal interface.[25] The development of a coordinate bond is caused by the transfer of π-density of molecular electrons from inhibitor molecules to open d-orbitals at the electrode surface, which is the basis of the chemisorption mechanism.

Arrhenius diagrams for C-steel deterioration in sweet oilfield environments with the lack and existence of H1, H2, and H3 inhibitors are presented in Figure 9A. Based on the Arrhenius model, the obvious activation energy (E_a) and i_{cor} are connected by the following equation:[45]

$$\log i_{cor} = \log A - \left(\frac{E_a}{2.303R}\right)\left(\frac{1}{T}\right) \tag{11}$$

where R, T, and A are the general gas constant, Kelvin temperature, and pre-exponential Arrhenius factor, respectively.[10] By comparing E_a in the blank and protected systems, considerable data about the mechanism of the Schiff base H1, H2, and H3 compounds' adsorption route could be discovered.

The straight line slope in Figure 9A is used to calculate the E_a values of blank and protected solutions, and the information is documented in Table 5. Generally, the greater E_a value found for the blank medium compared to the protected one designates the chemical adsorption process. This might be explained by a shift in the net deterioration path from exposed surfaces to places that have been adsorbed, which refers to a considerable decrease in E_a at an improved degree of the protected process.[50] The outcomes in Table 5 show that E_a values for H1, H2, and H3 Schiff base compounds (E_a = 18.93, 17.34, and 12.63 kJ mol^{-1}) were lower than that for the blank system (E_a = 24.82 kJ mol^{-1}). The overlapping of the electron density of the reacting molecules of the current Schiff bases to the valence shell of unfilled d-orbitals of iron species surface, which interferes with the anodic process of a degradation reaction, validates the chemical adsorption mechanistic pathway *via* the formation of a coordination bond.

Furthermore, additional activation thermodynamic indices of the corrosive route, for example, the entropy and enthalpy of activation ($\Delta H^*$and ΔS^*), were calculated from the transition-state equation:[51]

https://doi.org/10.1021/acsomega.3c00561
ACS Omega 2023, 8, 11512−11535

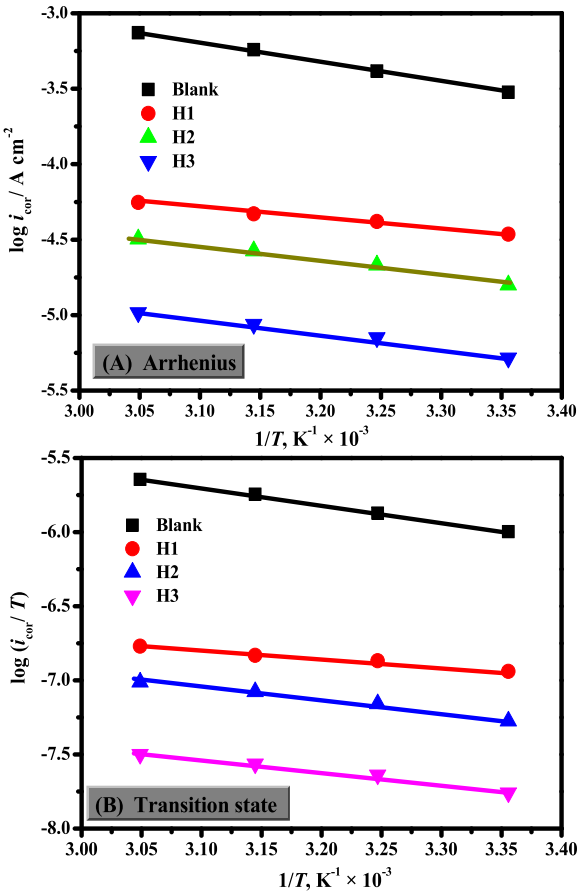

Figure 9. (A) Arrhenius and (B) transition state plots for C-steel deterioration in sweet oilfield environments in the absence and existence of H1, H2, and H3.

$$\log\left(\frac{i_{cor}}{T}\right) = \left[\log\left(\frac{R}{Nh}\right) + \left(\frac{\Delta S^*}{2.303R}\right)\right] - \left(\frac{\Delta H^*}{2.303R}\right)\left(\frac{1}{T}\right) \quad (12)$$

where h characterizes Planck's constant and N describes Avogadro's number. A diagram of $\log(i_{cor}/T)$ vs $1/T$ for C-steel corrosion in saturated solutions of NaCl with CO_2 in the lack and existence of H1, H2, and H3 Schiff base compounds is depicted in Figure 9B. The slope $[-\Delta H^*/(2.3030R)]$ and intercept $[\log(R/hN) + \Delta S^*/(2.3030R)]$ of these lines are computed. The $\Delta S^*$and ΔH^* values are shown in Table 5. The ΔH^* and E_a values are comparable in proximity and share the same aesthetic. This is in accordance with the transition-state model. The endothermic properties of the steel corrosion are indicated by the positive ΔH^* values.[52] In the inhibited system, this has also been said to be a sign of postponed C-steel corrosion. The three additive molecules (H1, H2, and H3 Schiff base compounds) have negative ΔS^* values, showing that the association phenomena rather than the dissociation phenomenon are used to determine the rate at which the started complex is formed.[53] Accordingly, it was found that the occurrence of H3 has a greater negative ΔS^* than H1 and H2 molecules (Table 5). This could be interpreted as H3 having a larger molecular weight, which causes a more pronounced fall in disruption upon the formation of the activated complex. Moreover, the noticed increase of ΔS^* is evocative of water molecules replaced through the adsorption of the Schiff bases H1, H2, and H3 on the steel interface.[54]

3.3. Adsorption Considerations. For the adsorption process of the current compounds on the steel interface, the mechanism of Schiff base molecules' corrosive prevention for C-steel in sweet oilfield environments may be understood. Models based on adsorption isotherms provide information on the interactions between the metal and the inhibitor. The H1, H2, and H3 molecules' effectiveness as corrosion inhibitors may be explained by the fact that donor atoms, *i.e.*, N (nitrogen) and O (oxygen), are found in the molecular constructions of the examined Schiff base derivatives, which favor superior adsorption on the C-steel interface. Several isotherms, such as the Temkin, Frumkin, Freundlich, and Langmuir models, have been utilized to characterize the mode of adsorption processes of the Schiff base derivatives on the C-steel substrate. The models of adsorption isotherms are expressed in the following equations:[55]

$$\text{Freundlich;}\ \Rightarrow\Rightarrow \log\theta = \log K_{ads} + n\log C_{inh.} \quad (13)$$

$$\text{Frumkim;}\ \Rightarrow\Rightarrow \ln\left[\frac{\theta}{(1-\theta)C_{inh.}}\right] = \ln K_{ads} + 2\alpha\theta \quad (14)$$

$$\text{Temkin;}\ \Rightarrow\Rightarrow \exp^{(2\alpha\theta)} = K_{ads}C_{inh.} \quad (15)$$

$$\text{Langmuir;}\ \Rightarrow\Rightarrow \frac{C_{inh.}}{\theta} = \frac{1}{K_{ads.}} + C_{inh.} \quad (16)$$

where K_{ads} denotes the equilibrium-adsorption constant, C_{inr} designates the Schiff base concentration in mol/L, and θ is the part surface of coverage. The regression coefficient (R^2) was used to choose the best appropriate isotherm model out of all those that were tried. With all linear R^2 values close to unity, the Langmuir isotherm was determined to be the mode that best fit experimental results, showing that the adsorption process on the f H1, H2, and H3 on C-steel in the investigated corrosive media followed the Langmuir isotherm model. The model of Langmuir adsorption considered as C_{inh}/θ vs C_{inh} is presented in Figure 10, where the straight-line slope is nearly unity (S = 1.06, 1.02, and 1.01 for H1, H2, and H3, respectively) and the intercept equals ($1/K_{ads}$), demonstrating that the best match is provided by Langmuir adsorption.[56] Understanding the mechanistic pathway of the mitigation process requires knowledge of thermodynamic parameters. The degree of standard free energy (ΔG^0_{ads}) is derived by[57]

Table 5. Thermodynamic Activation Strictures for C-Steel Deterioration in the Blank Sweet Oilfield Environment and with Addition of 0.5 mmol/L H1, H2, and H3

corrosion systems	E_a (kJ mol^{-1})	ΔH^* (kJ mol^{-1})	ΔS^* (J mol^{-1} k^{-1})	K_{ads} (L mol^{-1})	ΔG^0_{ads} (kJ mol^{-1})
blank medium	24.82	22.65	−287.23		
H1	18.93	16.13	−345.51	8.87×10^4	−41.38
H2	17.34	13.89	−387.32	10.86×10^4	−41.92
H3	12.63	11.76	−421.76	12.98×10^4	−42.41

https://doi.org/10.1021/acsomega.3c00561
ACS Omega 2023, 8, 11512−11535

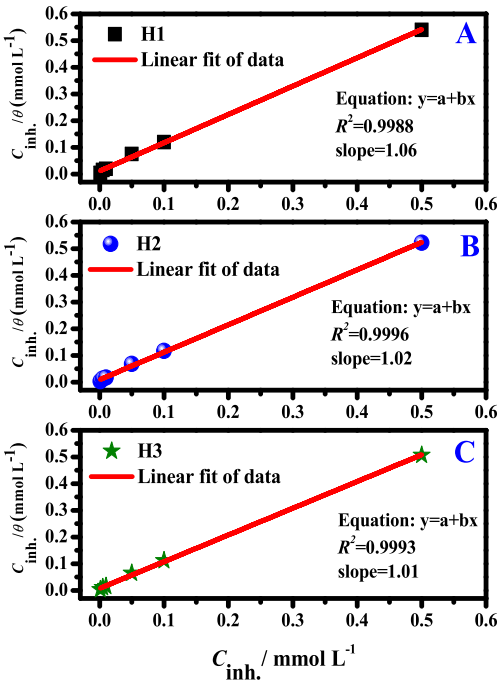

Figure 10. Langmuir isotherm of H1 (A), H2 (B), and H3 (C) adsorption at the C-steel/solution interface using the PDP technique at 55 °C.

$$\Delta G^{o}_{ads} = -RT\ln(55.5 \times K_{ads}) \quad (17)$$

The ΔG^{0}_{ads} values are usually exploited to approve the adsorption category between the Schiff base derivatives and C-steel interface.[58] The physisorption resulting from the electrostatic attraction between the steel substrate and charged inhibitor species is confirmed by the value of ΔG^{0}_{ads} up to −20 kJ mol^{-1}. While ΔG^{0}_{ads} value ≤ to −40.0 kJ mol^{-1}, chemisorption is indicated by charge transference from the Schiff base compounds to the C-steel interface through a coordination bond.[59] It is known that a combination of chemisorption and physisorption occurs between −20 and −40 kJ mol^{-1}. The ΔG^{0}_{ads} values detailed in this investigation (Table 5) are −41.38, −41.92, and −42.41 kJ mol^{-1} for H1, H2, and H3 compounds, respectively. These disclose that the adsorbing system of the prepared CH═N compounds on the C-steel interface is chemisorption.[51]

3.4. Corrosion Mitigation Mechanism. The mechanisms of steel's CO_2 corrosion are intricate. CO_2 has been shown to have two impacts.[60] First, despite the solution's acidity, there was a stronger cathodic development of hydrogen (this influence is supplementary with the buffering characteristics of carbonic acid). Second, the low solubility of iron carbonate is associated to the development of carbonate layers at the anodic steel surface. Depending on eq 18, CO_2 gas dissolves in water and undergoes hydration to generate a "weak" carbonic acid.

$$CO_{2(g)} \leftrightarrow CO_{2(aq)};\ CO_{2(aq)} + H_2O \leftrightarrow H_2CO_{3(aq)} \quad (18)$$

The H_2CO_3 then disassociates into HCO_3^- and CO_3^{2-}as displayed in eq 19:

$$H_2CO_{3(aq)} \leftrightarrow H^+ + HCO_3^- \leftrightarrow H^+ + CO_3^{2-} \quad (19)$$

Carbon dioxide deterioration is an electrochemical process within a general reaction specified in eq 20:

$$Fe + CO_2 + H_2O \leftrightarrow FeCO_3 + H_2 \quad (20)$$

$FeCO_3$ is a corrosion byproduct of CO_2 corrosion that, depending on the ambient factors, when precipitated may produce either a protective scale or a nonprotective scale.

Corrosion inhibition relies on the enhancement of a protecting/adsorbed coating film on the steel surface and involves a complicated mechanism. Adsorption is controlled by a variety of variables, and it largely refers to the following elements: interactions among inhibitors and their substrates, incorporation of the inhibiting agent into the surface layer, electrode potentials, inhibitor concentrations, chemical reactions, temperature, and characteristics of the consistent surface, among others.[61] The donor−acceptor attractions between the oxygen and nitrogen atoms and the unoccupied d orbitals of the steel substrate atoms can directly lead to the adsorbing action of the investigated CH═N compounds on the metal surface. Considerably, such molecules are found on the metal surface by the electron-donating groups such as carboxyethyl imino groups, nitrogen, sulfur, and oxygen atoms, and aromatic rings through the adsorption action.

It is well recognized that such compounds with organic moieties start their protective function by adhering to the C-steel/solution interface with additional molecules. The chemical nature of the substance, the charge sharing throughout the entire inhibitor molecule, the nature, and the charged C-steel interface all have an impact on the adsorption approach. Generally, a different method of adsorption between the C-steel interface and Schiff base molecules is not possible because of the complexity of a specific inhibitor's inhibition and adsorption. As a result, two methods of adsorption may frequently be of importance. There are two ways that the H1, H2, and H2 Schiff base molecules can bind to the C-steel surface. The first method is physical adsorption, where O (oxygen) and N (nitrogen) atoms in the inhibitor assembly and the anodic and cathodic regions of the C-steel interface are attracted to one another by electrostatic forces. The second method uses chemical adsorption, in which water molecules from the C-steel contact are replaced and electrons from the N and the delocalized π-electrons of the aryl moiety are transferred to iron. Accordingly, the molecules H1, H2, and H3 (Schiff base derivatives) might bind to the C-steel surface as a result of accepting−donating interactions of the unoccupied d orbitals of the iron surface with the benzene rings' π-electrons. The inhibition effectiveness accomplished by H1, H2, and H3 (Schiff base derivatives) may be due to a blend of chemical and physical adsorption, with a preference for the second type. Figure 11 displays the schematic exemplification of adsorption of the H1 inhibitor over the C-steel surface.

3.5. Surface Morphology by FE-SEM and EDAX Characterization. SEM morphologies and EDAX surface analysis for C-steel in CO_2-saturated brine were completed in the lack and occurrence of 1×10^{-6} and 5×10^{-4} M H1, H2, and H3. Figure 12a shows an SEM micrograph of a blank metal surface. The depiction displays the luminosity of the steel interface without any impurities. Figure 12b shows an SEM picture of the steel specimen after being exposed in the brine solution (3.5%) saturated with CO_2 without an inhibitor. It is obvious that the surface is robustly affected because of the attack by species like HCO_3^- and H^+ and a porous-like surface has been formed, leading to the formation of $FeCO_3$ layers that are not protective and the appearance of high roughness. In addition, the occurrence of the corrosion layer was gray to black,

https://doi.org/10.1021/acsomega.3c00561
ACS Omega 2023, 8, 11512−11535

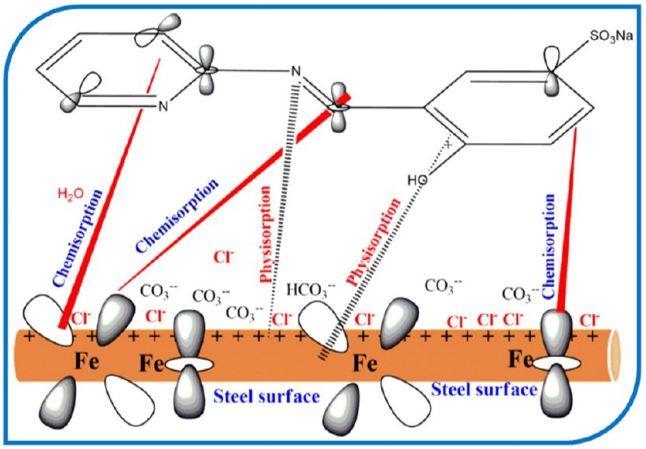

Figure 11. Adsorption mechanism of H1 inhibitor over C-steel.

representative of Fe_3C layers.[62] In the occurrence of 1×10^{-6} M H1 (Figure 12c), 1×10^{-6} M H2 (Figure 12e), and 1×10^{-6} M H3 (Figure 12g), respectively, the coarse surface is clearly reduced, demonstrating the development of a layer on the steel interface. At higher inhibitor doses of 5×10^{-4} M H1, H2, and H3 (Figure 12d,f,h), the surface was free from corrosion, and it was very smooth and more protected. Thus, it can be decided from Figure 12c−h that in the occurrence of the studied inhibitors, the corrosion does not occur, and the inhibitor species has a robust inclination to adsorb on the metal surface, protecting it from the aggressive medium.

To further comprehend the chemical nature of the carbon steel/inhibitor interface, EDAX analysis was performed. Figure 13a shows an EDAX spectrum for pure carbon steel surface before immersion. The featured peaks are due to metals existing in the metal (Fe, Mn, Cr, and C). EDAX analysis of the corrosion products in the aggressive blank solution (uninhibited) was performed at different sites, and the corresponding

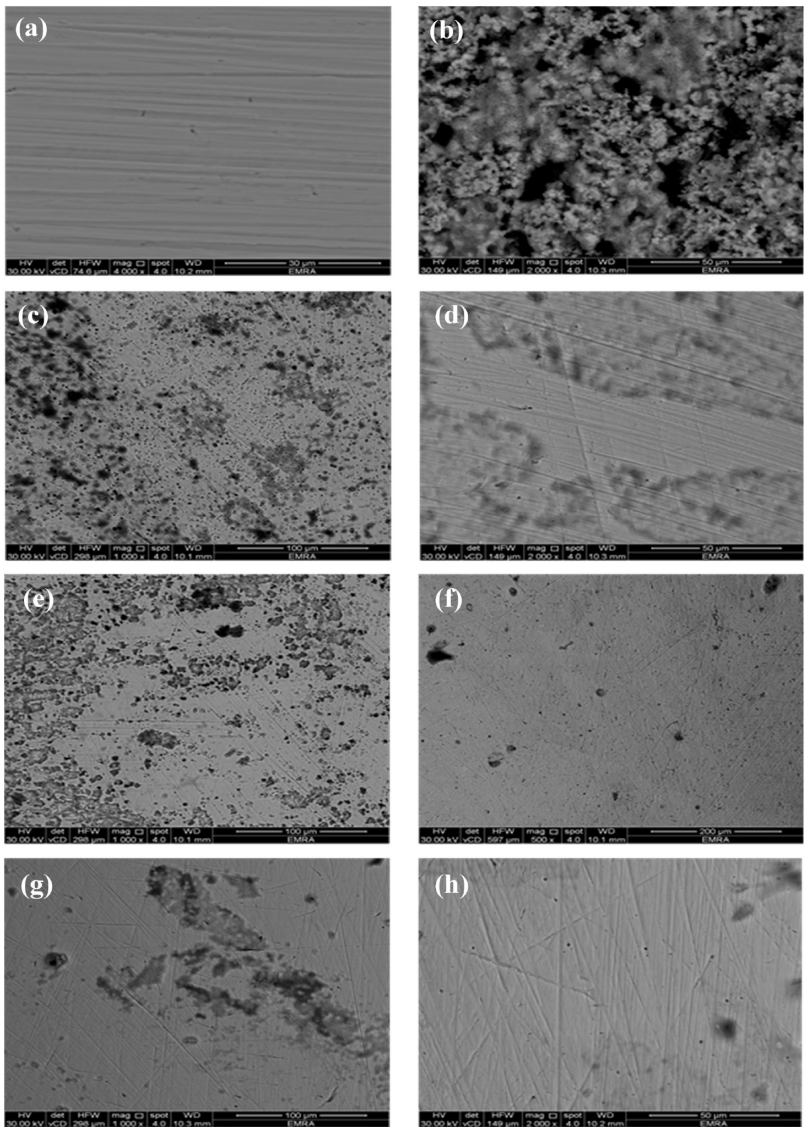

Figure 12. SEM micrograph of C1018-steel electrode surface and after immersion in CO_2-saturated brine containing different concentrations of H1, H2, and H3 for 72 h. (a) Blank C-steel, (b) in CO_2-saturated brine, (c) in CO_2-saturated brine + 1×10^{-6} M H1, (d) in CO_2-saturated brine + 5×10^{-4} M H1, (e) in CO_2-saturated brine + 1×10^{-6} M H2, (f) in CO_2- saturated brine + 5×10^{-4} M H2, (g) in CO_2-saturated brine + 1 × 10−6 M H3, and (h) in CO_2-saturated brine + 5×10^{-4} M H3.

https://doi.org/10.1021/acsomega.3c00561
ACS Omega 2023, 8, 11512−11535

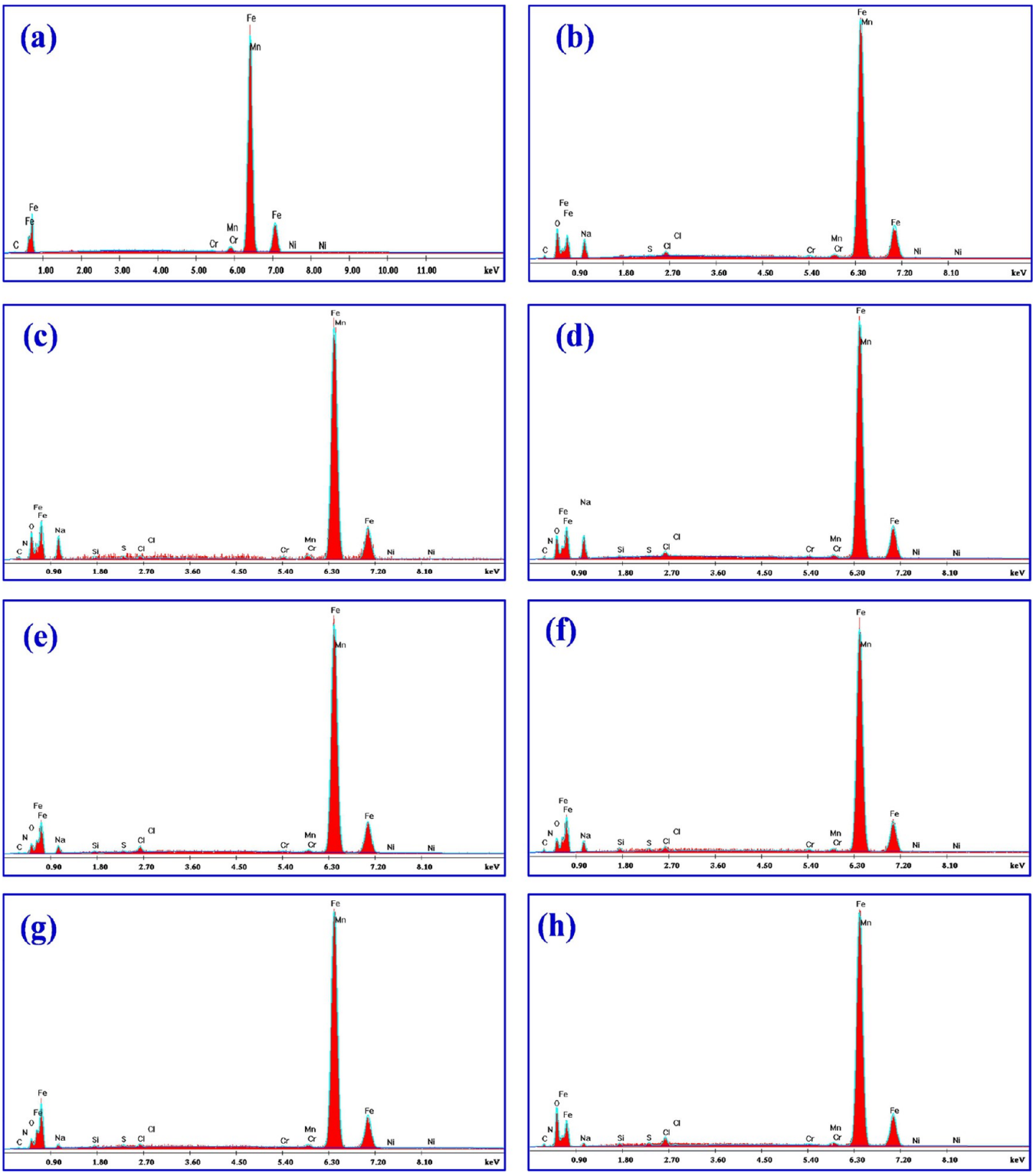

Figure 13. EDAX spectrum of C1018-steel electrode surface and after immersion in CO_2-saturated brine containing different concentrations of H1, H2, and H3 for 72 h. (a) Blank C-steel, (b) in CO_2-saturated brine, (c) in CO_2-saturated brine + 1×10^{-6} M H1, (d) in CO2-saturated brine + 5×10^{-4} M H1, (e) in CO_2-saturated brine + 1×10^{-6} M H2, (f) in CO_2-saturated brine + 5×10^{-4} M H2, (g) in CO_2-saturated brine + 1×10^{-6} M H3, and (h) in CO_2-saturated brine + 5×10^{-4} M H3.

element contents are displayed in Figure 13b. The findings indicate that Fe partially decreased and the corrosion products consisted of Fe, Cl, C, and O elements. The occurrence of the O and Cl^- ions may be related to the presence of Fe_3O_4 and $FeCl_2$ as corrosion products.[63] In the lack of O_2, EDAX analysis elucidates the existence of $FeCO_3$ film. The spectrum in the aggressive medium comprising diverse concentrations of H1, H2, and H3 inhibitors also shows increased C, O, and N atoms (the elements present in the inhibitor molecules) and decreased Fe percent (Figure 13c–h), indicating that the surface is coated

https://doi.org/10.1021/acsomega.3c00561
ACS Omega 2023, 8, 11512−11535

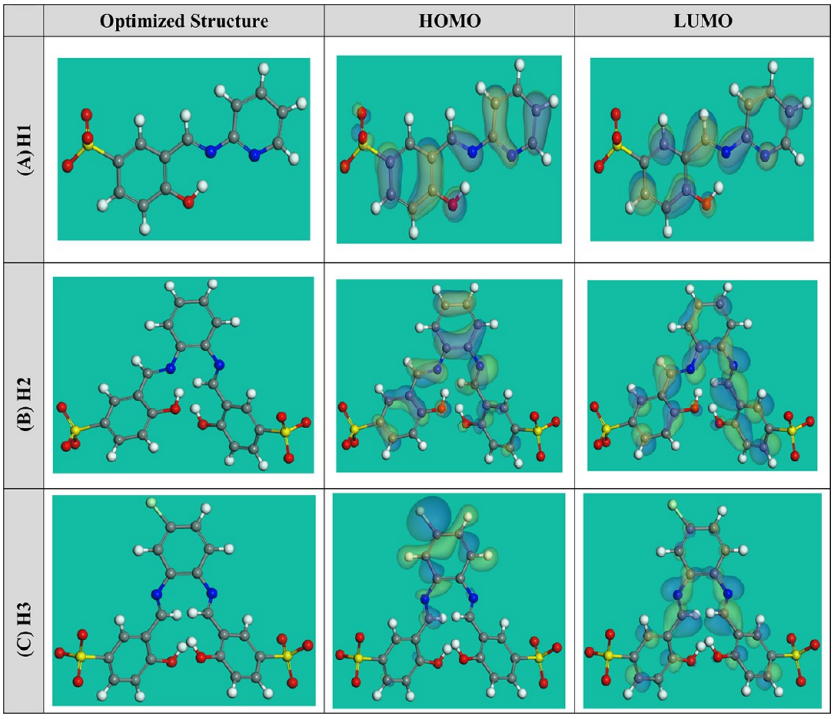

Figure 14. Optimized structure and HOMO and LUMO orbital occupation for the investigated Schiff base derivatives (A) H1, (B) H2, and(C) H3 molecules using the DFT method.

with an inhibiting compound layer. Moreover, the N peaks are increased by increasing the inhibitor dose, which designated that the inhibiting species are adsorbed on the metal surface and prohibit the surface from extra corrosion.

3.6. DFT Calculations. According to Figure 14, the molecules of the protonated Schiff base derivatives have optimal structures and LUMO and HOMO distributions, and the relevant theoretical characteristics are listed in Table 6.

Table 6. DFT Parameters of the Schiff Base Derivative Molecules

parameters	H1	H2	H3
E_{HOMO} (eV)	−5.23	−4.64	−4.23
E_{LUMO} (eV)	−2.54	−2.76	−2.91
$\Delta E = E_{LUMO} - E_{HOMO}$ (eV)	2.69	1.88	1.31
electronegativity (χ)	3.89	3.70	3.57
global hardness (η)	1.35	0.94	0.66
global softness (σ)	0.74	1.06	1.52
global electrophilicity index (ω)	5.61	7.27	9.70
the number of electrons transferred (ΔN)	1.16	1.75	2.61
$\Delta E_{back\text{-}donation}$	−0.34	−0.24	−0.16
dipole moments (μ) Debye	17.87	18.09	19.43
molecular surface area, Å^2	279.22	429.09	474.75

According to the FMO theory, LUMO and HOMO energies serve to identify the capability of donor or acceptor interactions carried out at the surface of the additive/metal.[64] Therefore, for an inhibitor molecule with high E_{HOMO} and low E_{LUMO} values, the corrosion inhibition proficiency is increased. In comparison to H1 and H2 (−5.23 and −4.64 eV) molecules, the H3 molecule has a maximum E_{HOMO} value of −4.23 eV, as seen in Table 6. As shown in Figure 14, the HOMO level was clearly put on the pyridinium, imine moieties, and benzene rings for the additive molecules, indicating that these sites are preferred for electrophilic assaults on the steel interface. These descriptions support the ability of the inhibitor additive to adsorb on the steel contact, leading to an increase in protection effectiveness that was well in line with the practical results. However, compared to H1 and H2 molecules (−2.54 and −2.76 eV), the E_{LUMO} value for the H3 molecule is lower at −2.91 eV (Table 6). The greater protective power of the H3 molecule is indicated by its lower E_{LUMO} value, which is consistent with earlier studies.

Similarly, the energy gap (ΔE) is a crucial stricture to strengthen the corrosion protection ability of the additive molecule, which upsurges as the ΔE value is diminished.[65] As recorded in Table 6, the H3 compound has a slighter ΔE value (1.31 eV) than H1 and H2 molecules (2.69 and 1.88 eV), which improves the superior inclination of H3 compounds to be adsorbed on the steel surface.

Most inhibitors typically have relatively low values for electronegativity (χ), which represents the inhibitor's ability to contribute electrons to the surface of steel.[66] Contrarily, high values of electronegativity (χ) also present a great possibility for inhibitor molecules to acquire electrons from steel interface atoms (*i.e.*, back-donation) and form a more durable bond with metal interface.[67] As established in Table 6, the H3 compound has a smaller ΔE value (3.57 eV) than H1 and H2 additives (3.89, 3.70 eV), which enhances the superior inclination of the H3 compound to contribute electron to the steel interface and form adsorbed protective film.

Furthermore, the stability and reactivity of the compounds could be evaluated from hardness (η) and softness (σ); *i.e.*, soft compounds have protection capability greater than that of hard compounds by the smooth transfer of electrons to the metal surface by the adsorption, so they perform as effective corrosion additives.[68] Table 6 shows that compared to H1 and H2 molecules, the H3 molecule has higher softness values and lower hardness values, which describe smoothly devoted electrons to the metal substrate and excellent inhibitory properties.

https://doi.org/10.1021/acsomega.3c00561
ACS Omega 2023, 8, 11512−11535

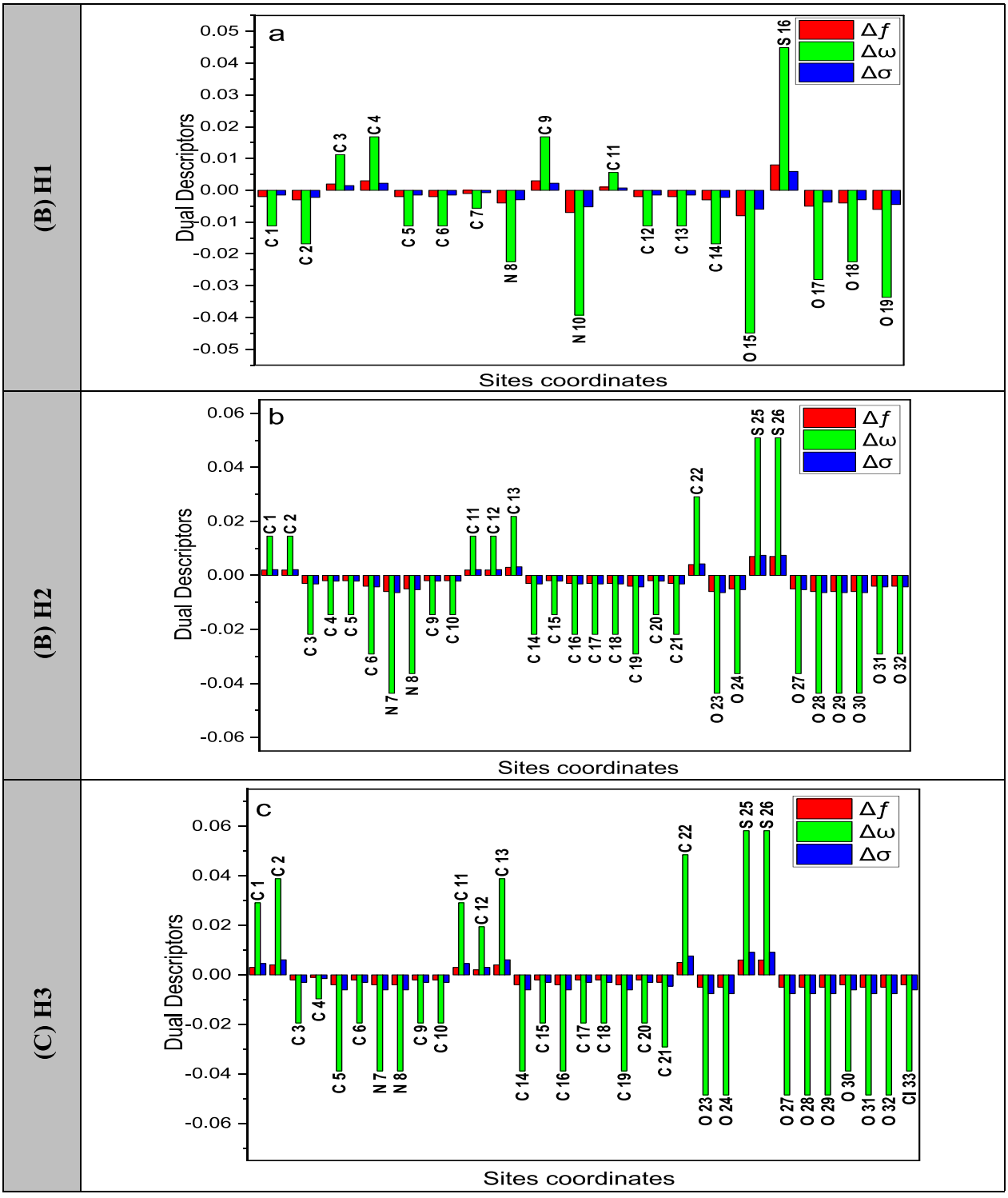

Figure 15. Graphical representation of the dual descriptors (Δf, $\Delta\sigma$, and $\Delta\omega$) for the maximum active sites of the investigated Schiff base derivatives (A) H1, (B) H2, and (C) H3 molecules using the DFT method.

The inhibitor's ability to donate or absorb electrons is also determined by the fraction of electron transfer and the $\Delta E_{\text{back-donation}}$ parameter. The electron transfer from the inhibitor to the atoms of the steel interface is therefore likely if the ΔN values are more than zero, whereas the electron transfer from the metal atoms to the inhibitor molecule is feasible if the ΔN values are less than zero (*i.e.*, back-donation).[69] The fact that the studied compounds have ΔN values greater than zero, as shown in Table 6, indicates that Schiff base derivatives are sufficiently capable of contributing electrons to the metal surface. Additionally, the $E_{\text{back-donation}}$ will be <0 when $\eta > 0$, and this is dynamically desired. An electron is removed from a molecule and tracked by a back-donation from the molecule.[70] The values of $E_{\text{back-donation}}$ for Schiff base derivative compounds in Table 6 are negative, indicating that back-donation is desirable for the molecules and creates a strong connection.[71]

https://doi.org/10.1021/acsomega.3c00561
ACS Omega 2023, 8, 11512−11535

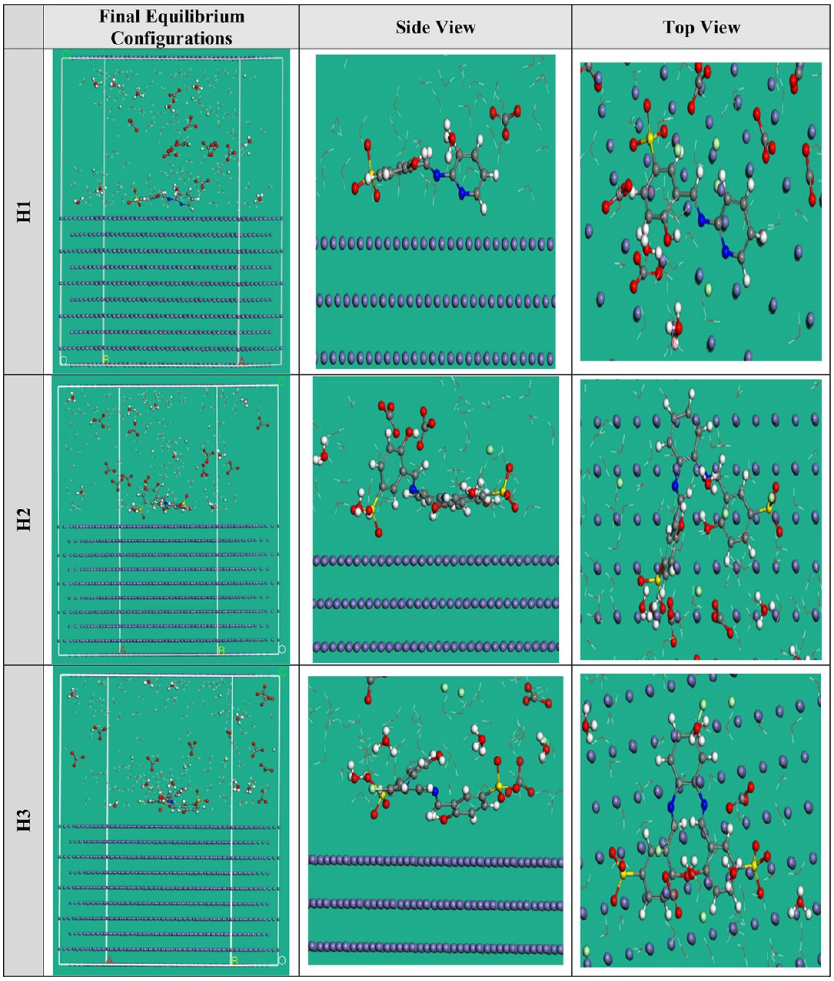

Figure 16. The highest proper adsorption arrangement for the Schiff base derivative molecules on the Fe (110) substrate achieved by the adsorption locator module.

The dipole moment is a risky characteristic that favors the prognosis pathway of corrosion inhibition as well.[72] Increased distortion energy and molecule adsorption on the metal surface are both benefits of increased dipole moment. As a result, the ability to inhibit corrosion is improved because of the increase in dipole moment.[73] According to Table 6, the H3 molecule has a higher dipole moment value than the H1 and H2 molecules (17.87 and 18.09 Debye, respectively), which permits a greater propensity for the H3 molecule to be adsorbed on the metal surface and increase the inhibition.

Additionally, the molecular surface area of inhibitor species is proportional to their tendency to protect the steel surface in the aggressive media. Because of an increase in the contact area between the inhibitor molecules and the steel surface, the protection effectiveness increases as the molecular structure size increases. The H3 molecule exhibits more molecular surface area (474.75 Å2) than H1 and H2 molecules (279.22 and 429.09 Å2), and as a result, the H3 molecule has greater protective ability than other Schiff base derivatives molecules, as shown in Table 6.

The local reactivity of the Schiff base compounds can be evaluated by computing the Mulliken atomic charges, dual descriptors (Δf_k, $\Delta\sigma_k$, and $\Delta\omega_k$), local electrophilicity ($\omega_k^{\pm}$), local softness descriptor ($\sigma_k^{\pm}$), and Fukui indices (f_k^{+}andf_k^{-}) from the following equations:[74]

$$\sigma_k^{\pm} = \sigma f_k^{\pm} \tag{21}$$

$$\omega_k^{\pm} = \omega f_k^{\pm} \tag{22}$$

$$\Delta f_k^{\pm} = f_k^{+} - f_k^{-} \tag{23}$$

$$\Delta\sigma_k = \sigma_k^{+} - \sigma_k^{-} \tag{24}$$

$$\Delta\omega_k = \omega_k^{+} - \omega_k^{-} \tag{25}$$

For interpretation, the most significant findings are demonstrated in Table S1. The assessed Fukui indices (Table S1) distinguished for the inhibitor molecule ascribe the positions by which the Schiff base molecules will be adsorbed onto the iron substrate. f_k^{-} describes the electrophilic attack reactivity (donation centers), whereas f_k^{+} indicates the nucleophilic attack reactivity centers (accepting sites).[75] The premier f_k^{+} for C1−C3,C5, C7, N8, C9, N10, C11−C14, O15, S16, and O17−19 for H1; C1, N8, C10, C17, C18, C22, O23, S25, S26, and O27−32 for H2; and C5, N7, N8, C13, C17, S25, S26, O27−33, and Cl33 for H3 describes the center for electron contribution. The highest f_k^{-} is found at C1−C3,C5, C7, N8, C9, N10, C11−C14, O15, S16, and O17−19 for H1; C3, C6, N8, C10, C14, C15, C17, C18, C20, C21, C22, O23, S25, S26, and O27−32 for H2; and C5, C6, N7, N8, C14, C17, C18, O23, O24, S25, S26, O27−33, and Cl33 for H3, revealing the

https://doi.org/10.1021/acsomega.3c00561
ACS Omega 2023, 8, 11512−11535

Table 7. Data and Descriptors Computed by the MC Simulations for the Adsorption of the Schiff Base Derivatives Molecules on Fe (110)

corrosion systems	adsorption energy (kcal mol^{-1})	rigid adsorption energy (kcal mol^{-1})	deformation energy (kcal mol^{-1})	dE_{ads}/dN_i: inhibitor (kcal mol^{-1})	dE_{ads}/dN_i: hydronium (kcal mol^{-1})	dE_{ads}/dN_i: carbonate ions (kcal mol^{-1})	dE_{ads}/dN_i: chloride ions (kcal mol^{-1})	dE_{ads}/dN_i: water (kcal mol^{-1})
Fe (110) H1 water hydronium carbonate ions chloride ions	−3058.24	−1623.53	−1434.71	−214.20	−57.33	−85.23	−106.02	−16.18
Fe (110) H2 water hydronium carbonate ions chloride ions	−3090.64	−1645.42	−1445.23	−221.16	−57.17	−85.81	−106.80	−16.27
Fe (110) H3 water hydronium carbonate ions chloride ions	−3158.28	−1698.88	−1459.41	−232.59	−57.25	−86.92	−107.88	−16.22

capability for a back-donation.[76] A further measure of a molecule's local reactivity is its Mulliken atomic charge, which is shown in Table S1 for the molecules H1, H2, and H3. Higher-negative-charged atoms, which resemble electron donors (nucleophilic sites).[77] Consequently, the atoms C1, C2, C5−7, N8, N10, C12−C14, O15, and O17−O19 for H1; C3−C6, N7, N8, C9, C10, C14−21, O24, and O27−O32 for H2; and C3−C6, N7, N8, C9, C10, C14−21, O23, O24, O27-O32, and Cl33 for H3 are efficient centers located on benzene rings, oxygen and nitrogen atoms having the ability of contributing electrons as they interrelate with the steel interface. The local dual descriptors are additionally more accurate and comprehensive tools than the Fukui indices (f_k^+andf_k^-) and the local electrophilicity ($\omega_k^{\pm}$) and softness ($\sigma_k^{\pm}$); the dual local descriptors of the most prominent example active spots are graphically displayed in Figure 15. The gained consequences display that the centers with the Δf_k, $\Delta\sigma_k$, and $\Delta\omega_k < 0$ have a tendency to relocate an electron to the metal surface. By contrast, those centers with Δf_k, $\Delta\sigma_k$, and $\Delta\omega_k > 0$ have to ability to accept an electron from the metal. As can be distinguished in Figure 15, the highest efficient sites for electron donation are at C1, C2, C5−7, N8, N10, C12−C14, O15, and O17−O19 for H1; C3−6, N7, N8, C9, C10, C14−C21, O23, O24, and O27−O32 for H2; and C3−6, N7, N8, C9, C10, C14−C21, O23, O24, O27−O32, and Cl33 for H3, whereas the efficient accepting sites are at C3, C4, C9, C11, and S16 for H1; C1, C2, C11, C12, C13, C22, S25, and S26 for H2; and C1, C2, C11, C12, C13, C22, S25, and S26 for H3.

3.7. MC Simulations. In addition to providing a clear notion for the adsorption mechanism, MC simulations were used to identify the attractions of the inhibitor species with the steel surface. As a result of the adsorption locator module's roughly flat disposition, Figure 16 shows the highest proper adsorption formations for the Schiff base derivative molecules on the steel interface in acidic solutions, indicating an improvement in the adsorption and maximum surface coverage.[78] Additionally, Table 7 reveals the calculated results for the adsorption energies from the MC simulations. It was discovered that the H3 molecule (−3158.28 kcal mol^{-1}) has a higher negative adsorption energy value than the H1 and H2 molecules (−3058.24 and −3090.64 kcal mol^{-1}). This result is consistent with the experimental results and assumes that the energetic adsorption of the H3 molecule on the steel interface creates a stable adsorbed film and protects the steel from corrosion.[28] Additionally, Table 7 shows that the adsorption energy value for the H3 molecule for the pre-geometry optimization step is unrelaxed (−1698.88 kcal mol^{-1}), which is more negative than those of H1 and H2 molecules (−1623.53 and −1645.42 kcal mol^{-1}), and that for the post-geometry optimization step is relaxed (−1459.41 kcal mol^{-1}), which is greater than those for H1 and H2 molecules (−1434.71 and −1445.23 kcal mol^{-1}), confirming a higher inhibition capability for the H3 compound than H1 and H2 molecules.

The dE_{ads}/dN_i values clarify the steel/adsorbate arrangement energy if the adsorbed additive molecule or other species has been excluded.[79] The dE_{ads}/dN_i value for both forms of H3 compound (−232.59 kcal mol^{-1}) is bigger than that for H1 and H2 compounds (−214.20 kcal mol^{-1}) as exposed in Table 7, which asserts the outstanding adsorption of the H3 compound compared to H1 and H2 compounds. Additionally, the dE_{ads}/dN_i values for hydronium ions, carbonate ions, chloride ions, and water molecules are low when compared to values for Schiff base derivative molecules, revealing a strong adsorption of inhibitor molecules over H_2O molecules, hydronium, chloride, and carbonate ions, enhancing the supersede of these ions. According to a combination of empirical and theoretical investigations, the molecules of the Schiff base derivatives are resolutely adsorbed on the steel surface and create a potent adsorbed defensive layer that results in corrosion protection for the steel surface in the corrosive medium.

3.8. Comparisons of the Inhibitory Capabilities of Some Conventional and Synthesized Corrosion Inhib-

https://doi.org/10.1021/acsomega.3c00561
ACS Omega 2023, 8, 11512−11535

Table 8. Comparisons of the Protective Effectiveness of Some Traditional Corrosion Inhibitors

inhibitor type	corrosive medium	inhibitor concentration	substrate type	adsorption isotherm & nature	inhibition capacity (%)	reference
chitosan Schiff base	3.5% NaCl + CO_2	150 ppm	J22 steel	Langmuir/mixed type	95.4%	79
O,O-dialkyl dithiophosphoric acid	CO_2-saturated brine	5 ppm	mild steel	Langmuir/mixed type	~70−96	80
amino triazole	CO_2 saturated 2.5% NaCl solution	4 mM	mild steel	Langmuir	~85−93.2	81
alkoxyphenyl substituents containing imidazolines	0.5 M NaCl saturated with CO_2	100 ppm	carbon steel	Langmuir	~96	82
2-mercaptobenzimi dazole	3.5% sodium chloride	800 ppm	mild steel	Langmuir	~54	83
amino acid Schiff base	CO2-saturated 3.5% NaCl solution	1.0 mM	carbon steel	Langmuir	91.44−96.53	25
H1	CO_2-saturated 3.5% NaCl	0.5 mM	C-steel	Langmuir/mixed type	96.5	present study
H2	CO_2-saturated 3.5% NaCl	0.5 mM	C-steel	Langmuir/mixed type	97.7	present study
H3	CO_2-saturated 3.5% NaCl	0.5 mM	C-steel	Langmuir/mixed type	98.1	present study

itors. The examination for innovative corrosion inhibitors that are also affordable and environmentally benign is continuously ongoing. For C-steel in a 3.5% sodium chloride medium saturated with CO_2, the Schiff base compounds based on phenylenediamine (0.5 mM) showed a high inhibitory capability of between 96.5 and 98.1% as shown in Table 8. The anticorrosive properties of several synthetic inhibitors on steel were investigated in a CO_2-NaCl medium utilizing weight loss and electrochemical tests.[79−83]

In a CO_2-saturated solution of NaCl, Ansari et al.[79] investigated the chitosan Schiff base's ability to suppress steel electrode corrosion. The inhibition power of the Schiff base based-chitosan was 95.4%. Abd El-Lateef et al. reported on the amino acid Schiff base's ability to prevent the corrosion of carbon steel in a brine solution saturated with carbon dioxide. The greatest protective capability of the amino acid Schiff base compounds was 96.53% at 1.0 mM. Table 8 demonstrates that our synthesized Schiff base has significantly more inhibitory capabilities than the previously reported synthetic compounds.

The experimental results showed that H2 and H3 molecules have higher inhibition performance than the H1 molecule due to the presence of two functional groups of CH═N and two hydroxyl groups (OH) in their structures compared to one of each in the H1 molecule. Both groups could strongly enhance the adsorption to C1018-steel and obviously reduce the corrosion rate compared to H1. Moreover, the presence of the chloro-aryl substituent in H3 could indicate the higher reactivity of H3 than that of H2. The high electronegativity of the chloro-aryl substituent in H3 could strongly withdraw the electron density through the H3 molecule (Figure 14); however, it showed a promoted reactivity toward the anticorrosion ability over that of H2. The high electronegativity of the chloro-aryl substituent in H3 (ω = 9.70) could decrease the electron density for bonding and adsorption on the carbon steel surface, but it could enhance the polarity of H3, as observed from the DFT studies (Table 6). The modified polarity (depending on the dipole moment values) of H3 compared to that of H2 (18.09 Debye) increased the probability of a number of electron transfer ΔN for H3 with dipole moment = 19.43 Debye (2.61) over that of H2 (1.75) by promoting the interaction with the carbon steel surface, as given in Table 6. Furthermore, H3 molecules have the lowest energy gap, so it is easy for them to donate electrons to the metal surface, leading to the strong adsorption of H3 on the C1018-steel interface.

4. CONCLUSIONS

Three water-soluble different derivatives of Schiff bases, as mono- and di-Schiff bases, were synthesized from the condensed 2-aminopyridine, *o*-phenylenediamine, or 4-chloro-*o*-phenylenediamine with sodium salicylaldehyde-5-sulfonate as H1, H2, and H3, respectively. All Schiff bases were characterized by all possible spectroscopic methods (NMR and FTIR spectra) and also by elemental analyses and conductivity features. Through electrochemical tests, good corrosion inhibition efficacy against C-steel of mono- and di-Schiff bases was confirmed. At a dose of 0.5 mM, the Schiff base compounds showed a high inhibitory capability of between 96.5 and 98.1%. PDP polarization curves provide evidence that mono- and di-Schiff bases are mixed-type corrosion inhibitors that predominantly impede anode reactions on the steel surface. The corrosion inhibitors (mono- and di-Schiff bases) on the steel interface follow the Langmuir adsorption model and belong to the spontaneous chemical and physical adsorption process. After adding the Schiff base molecules, SEM/EDX analyses revealed a smoother electrode surface, indicating that a protective layer had been constructed to shield the steel surface from interaction with corrosive ions. The inhibitor species might be adsorbed on the metal interface in its active areas, according to the findings of quantum calculations, and the order of inhibition is H3 > H2 > H1. With a greater understanding of the various approaches for evaluating corrosion and corrosion inhibitors as well as benefits for the oil and gas industries, this methodical study may offer a way to create novel corrosion inhibitors.

CREDIT AUTHORSHIP CONTRIBUTION STATEMENT

H.M. Abd El-Lateef: Investigation, Supervision, Methodology, Resources, Formal analysis, Data curation, Funding acquisition, Writing-original draft, Writing-review & editing. W.M.A. Nasr: Investigation, Methodology, Resources, Formal analysis, Data curation, Writing-original draft, Writing-review & editing. M.M. Khalaf: Methodology, Formal analysis, Data curation, Writing-original draft, Writing-review & editing. A.E. Mohamed: Investigation, Supervision, Methodology, Data curation, Writing-original draft, Writing-review & editing. M.N. Rashed: Investigation, Supervision, Methodology, Data curation, Writing-original draft, Writing-review & editing. M.S.S. Adam: Investigation, Resources, Methodology, Formal analysis, Data curation, Writing-original draft, Writing-review & editing.

https://doi.org/10.1021/acsomega.3c00561
ACS Omega 2023, 8, 11512−11535

■ ASSOCIATED CONTENT

Supporting Information

The Supporting Information is available free of charge at https://pubs.acs.org/doi/10.1021/acsomega.3c00561.

^{1}HMR of H1 in DMSO-d_6 at room temperature (Figure S1); ^{13}CMR of H1 in DMSO-d_6 at room temperature (Figure S2); and the evaluated Fukui indices (Table S1) (PDF)

■ AUTHOR INFORMATION

Corresponding Authors

Hany M. Abd El-Lateef − *Department of Chemistry, College of Science, King Faisal University, Al-Ahsa 31982, Saudi Arabia; Chemistry Department, Faculty of Science, Sohag University, Sohag 82524, Egypt;* orcid.org/0000-0002-6610-393X; Email: hmahmed@kfu.edu.sa, hany_shubra@science.sohag.edu.eg

Wafaa M. Abd El-Monem Nasr − *Chemistry Department, Faculty of Science, Aswan University, Aswan 81528, Egypt*; Email: wafaa.mahmoud9252@sci.aswu.edu.eg

Authors

Mai M. Khalaf − *Department of Chemistry, College of Science, King Faisal University, Al-Ahsa 31982, Saudi Arabia; Chemistry Department, Faculty of Science, Sohag University, Sohag 82524, Egypt*

Adila E. Mohamed − *Chemistry Department, Faculty of Science, Aswan University, Aswan 81528, Egypt*

Mohamed Nageeb Rashed − *Chemistry Department, Faculty of Science, Aswan University, Aswan 81528, Egypt*

Mohamed Shaker S. Adam − *Department of Chemistry, College of Science, King Faisal University, Al-Ahsa 31982, Saudi Arabia; Chemistry Department, Faculty of Science, Sohag University, Sohag 82524, Egypt;* orcid.org/0000-0001-8826-3558

Complete contact information is available at: https://pubs.acs.org/10.1021/acsomega.3c00561

Notes

The authors declare no competing financial interest.

■ ACKNOWLEDGMENTS

This work was supported through the Annual Funding track by the Deanship of Scientific Research, Vice Presidency for Graduate Studies and Scientific Research, King Faisal University, Saudi Arabia [grant 2197].

■ REFERENCES

(1) Abd El-Lateef, H. M.; Abdallah, Z. A.; Ahmed, M. S. M. Solvent-free synthesis and corrosion inhibition performance of Ethyl 2-(1,2,3,6-tetrahydro-6-oxo-2-thioxopyrimidin-4-yl) ethanoate on carbon steel in pickling acids: Experimental, quantum chemical and Monte Carlo simulation studies. *J. Mol. Liq.* **2019**, *296*, No. 111800.

(2) Khalaf, M. M.; Tantawy, A. H.; Soliman, K. A.; Abd El-Lateef, H. M. Cationic gemini-surfactants based on waste cooking oil as new 'green'inhibitors for N80-steel corrosion in sulphuric acid: A combined empirical and theoretical approaches. *J. Mol. Struct.* **2020**, *1203*, No. 127442.

(3) Wang, X.; Yang, H.; Wang, F. Inhibition performance of a gemini surfactant and its co-adsorption effect with halides on mild steel in 0.25 M H_2SO_4 solution. *Corros. Sci.* **2012**, *55*, 145−152.

(4) Yüce, A. O.; Kardaş, G. Adsorption and inhibition effect of 2-thiohydantoin on mild steel corrosion in 0.1 M HCl, Corrosion Science. 2012, *58*, 86−94, DOI: 10.1016/j.corsci.2012.01.013.

(5) Abd El-Lateef, H. M.; Alnajjar, A. O. Enhanced the protection capacity of poly (o-toluidine) by synergism with zinc or lanthanum additives at C-steel/HCl interface: A combined DFT, molecular dynamic simulations and experimental methods. *J. Mol. Liq.* **2020**, *303*, No. 112641.

(6) Mazumder, M. A. J. Synthesis, characterization and electrochemical analysis of cysteine modified polymers for corrosion inhibition of mild steel in aqueous 1 M HCl. *RSC Adv.* **2019**, *9*, 4277−4294.

(7) Alibakhshi, E.; Ghasemi, E.; Mahdavian, M.; Ramezanzadeh, B. Corrosion inhibitor release from Zn-Al-[PO_{43}-]-[CO_{32}-] layered double hydroxide nanoparticles. *Prog. Color, Color. Coat.* **2016**, *9*, 233−248.

(8) Singh, A.; Ansari, K. R.; Lin, Y.; Quraishi, M. A.; Lgaz, H.; Chung, I.-M. Corrosion inhibition performance of imidazolidine derivatives for J55 pipeline steel in acidic oilfield formation water: Electrochemical, surface and theoretical studies. *J. Taiwan Inst. Chem. Eng.* **2019**, *95*, 341−356.

(9) Abd El-Lateef, H. M.; Abu-Dief, A. M.; Mohamed, M. A. A. Corrosion inhibition of carbon steel pipelines by some novel Schiff base compounds during acidizing treatment of oil wells studied by electrochemical and quantum chemical methods. *J. Mol. Struct.* **2017**, *1130*, 522−542.

(10) Abd El-Lateef, H. M.; Abbasov, V. M.; Aliyeva, L. I.; Qasimov, E. E.; Ismayilov, I. T. Inhibition of carbon steel corrosion in CO_2-saturated brine using some newly surfactants based on palm oil: experimental and theoretical investigations. *Mater. Chem. Phys.* **2013**, *142*, 502−512.

(11) Alsabagh, A. M.; Migahed, M. A.; Awad, H. S. Reactivity of polyester aliphatic amine surfactants as corrosion inhibitors for carbon steel in formation water (deep well water). *Corros. Sci.* **2006**, *48*, 813−828.

(12) Mustafa, A. H.; Ari-Wahjoedi, B.; Ismail, M. C. Inhibition of CO_2 corrosion of X52 steel by imidazoline-based inhibitor in high pressure CO_2-water environment. *J. Mater. Eng. Perform.* **2013**, *22*, 1748−1755.

(13) Zhao, G.-x.; Lu, X.-h.; Xiang, J.-m.; Yong, H. A. N. Formation characteristic of CO_2 corrosion product layer of P110 steel investigated by SEM and electrochemical techniques. *J. Iron Steel Res., Int.* **2009**, *16*, 89−94.

(14) Ortega-Toledo, D. M.; Gonzalez-Rodriguez, J. G.; Casales, M.; Martinez, L.; Martinez-Villafañe, A. CO_2 corrosion inhibition of X-120 pipeline steel by a modified imidazoline under flow conditions. *Corros. Sci.* **2011**, *53*, 3780−3787.

(15) Linter, B. R.; Burstein, G. T. Reactions of pipeline steels in carbon dioxide solutions. *Corros. Sci.* **1999**, *41*, 117−139.

(16) Abbasov, V. M.; El-Lateef, H. M. A.; Aliyeva, L. I.; Ismayilov, I. T.; Qasimov, E. E.; Narmin, M. M. Efficient complex surfactants from the type of fatty acids as corrosion inhibitors for mild steel C1018 in CO_2-environments. *J. Korean Chem. Soc.* **2013**, *57*, 25−34.

(17) Obot, I. B.; Obi-Egbedi, N. O.; Umoren, S. A. Antifungal drugs as corrosion inhibitors for aluminium in 0.1 M HCl. *Corros. Sci.* **2009**, *51*, 1868−1875.

(18) Al-Shihry, S. S.; Sayed, A. R.; Abd El-lateef, H. M. Design and assessment of a novel poly (urethane-semicarbazides) containing thiadiazoles on the backbone of the polymers as inhibitors for steel pipelines corrosion in CO_2-saturated oilfield water. *J. Mol. Struct.* **2020**, *1201*, No. 127223.

(19) Nataraja, S. E.; Venkatesha, T. V.; Manjunatha, K.; Poojary, B.; Pavithra, M. K.; Tandon, H. C. Inhibition of the corrosion of steel in hydrochloric acid solution by some organic molecules containing the methylthiophenyl moiety. *Corros. Sci.* **2011**, *53*, 2651−2659.

(20) Verma, C.; Quraishi, M. A. Recent progresses in Schiff bases as aqueous phase corrosion inhibitors: Design and applications. *Coord. Chem. Rev.* **2021**, *446*, No. 214105.

(21) Hameed, A.; Al-Rashida, M.; Uroos, M.; Abid Ali, S.; Khan, K. M. Schiff bases in medicinal chemistry: a patent review (2010-2015). *Expert Opin. Ther. Pat.* **2017**, *27*, 63−79.

(22) Gupta, K. C.; Sutar, A. K. Catalytic activities of Schiff base transition metal complexes. *Coord. Chem. Rev.* **2008**, *252*, 1420−1450.
(23) Abd El-Lateef, H. M.; Ismael, M.; Mohamed, I. M. A. Novel Schiff base amino acid as corrosion inhibitors for carbon steel in CO_2-saturated 3.5% NaCl solution: experimental and computational study. *Corros. Rev.* **2015**, *33*, 77−97.
(24) Chakravarthy, M. P.; Mohana, K. N.; Pradeep Kumar, C. B. Corrosion inhibition effect and adsorption behaviour of nicotinamide derivatives on mild steel in hydrochloric acid solution. *Int. J. Ind. Chem.* **2014**, *5*, 1−21.
(25) Dao, V.-D.; Vu, N. H.; Choi, H.-S. All day Limnobium laevigatum inspired nano generator self-driven via water evaporation. *J. Power Sources* **2020**, *448*, No. 227388.
(26) Dao, V.-D. An experimental exploration of generating electricity from nature-inspired hierarchical evaporator: The role of electrode materials. *Sci. Total Environ.* **2021**, *759*, No. 143490.
(27) Abd El-Lateef, H. M.; Sayed, A. R.; Shalabi, K. Synthesis and theoretical studies of novel conjugated polyazomethines and their application as efficient inhibitors for C1018 steel pickling corrosion behavior. *Surfaces and Interfaces* **2021**, *23*, No. 101037.
(28) Dehghani, A.; Mostafatabar, A. H.; Bahlakeh, G.; Ramezanzadeh, B. A detailed study on the synergistic corrosion inhibition impact of the Quercetin molecules and trivalent europium salt on mild steel; electrochemical/surface studies, DFT modeling, and MC/MD computer simulation. *J. Mol. Liq.* **2020**, *316*, No. 113914.
(29) Feng, Y.; Chen, S.; Guo, W.; Zhang, Y.; Liu, G. Inhibition of iron corrosion by 5, 10, 15, 20-tetraphenylporphyrin and 5, 10, 15, 20-tetra-(4-chlorophenyl) porphyrin adlayers in 0.5 M H_2SO_4 solutions. *J. Electroanal. Chem.* **2007**, *602*, 115−122.
(30) Abd El-Lateef, H. M.; Shalabi, K.; Tantawy, A. H. Corrosion inhibition and adsorption features of novel bioactive cationic surfactants bearing benzenesulphonamide on C1018-steel under sweet conditions: Combined modeling and experimental approaches. *J. Mol. Liq.* **2020**, *320*, No. 114564.
(31) Adam, M. S. S.; Al-Omair, M. A.; Ullah, F. Catalytic comparison of various polar Zn (II)-and VO (II)-Schiff base complexes in (ep) oxidation processes of 1, 2-cyclohexene and cyclohexane. *Res. Chem. Intermed.* **2019**, *45*, 4653−4675.
(32) Reimann, M. J.; Salmon, D. R.; Horton, J. T.; Gier, E. C.; Jefferies, L. R. Water-soluble sulfonate Schiff-base ligands as fluorescent detectors for metal ions in drinking water and biological systems. *ACS Omega* **2019**, *4*, 2874−2882.
(33) Z., Wu; L., Zhou; Z., Jiang; D., Wu; Z., Li; X., Zhou, *Sulfonato−Cu (salen) Complex Catalyzed N-Arylation of Aliphatic Amines with Aryl Halides in Water*, Wiley Online Library, 2010. DOI: 10.1002/ejoc.201000840
(34) Mohamad, A.D.M.; El-Shrkawy, E.R.; Al-Hussein, M.F.I.; Adam, M.S.S. Water-soluble Cu (II)-complexes of Schiff base amino acid derivatives as biological reagents and sufficient catalysts for oxidation reactions. *J. Taiwan Inst. Chem. Eng.* **2020**, *113*, 27−45.
(35) Murmu, M.; Saha, S. K.; Bhaumick, P.; Murmu, N. C.; Hirani, H.; Banerjee, P. Corrosion inhibition property of azomethine functionalized triazole derivatives in 1 mol L^{-1} HCl medium for mild steel: Experimental and theoretical exploration. *J. Mol. Liq.* **2020**, *313*, No. 113508.
(36) Saha, S. K.; Dutta, A.; Ghosh, P.; Sukul, D.; Banerjee, P. Adsorption and corrosion inhibition effect of Schiff base molecules on the mild steel surface in 1 M HCl medium: a combined experimental and theoretical approach. *Phys. Chem. Chem. Phys.* **2015**, *17*, 5679−5690.
(37) Saha, S. K.; Murmu, M.; Murmu, N. C.; Banerjee, P. Evaluating electronic structure of quinazolinone and pyrimidinone molecules for its corrosion inhibition effectiveness on target specific mild steel in the acidic medium: a combined DFT and MD simulation study. *J. Mol. Liq.* **2016**, *224*, 629−638.
(38) Upadhyay, A.; Purohit, A. K.; Mahakur, G.; Dash, S.; Kar, P. K. Verification of corrosion inhibition of Mild steel by some 4-Aminoantipyrine-based Schiff bases−Impact of adsorbate substituent and cross-conjugation. *J. Mol. Liq.* **2021**, *333*, No. 115960.
(39) Farag, A. A.; Ali, T. A. The enhancing of 2-pyrazinecarboxamide inhibition effect on the acid corrosion of carbon steel in presence of iodide ions. *J. Ind. Eng. Chem.* **2015**, *21*, 627−634.
(40) Cao, S.; Liu, D.; Ding, H.; Wang, J.; Lu, H.; Gui, J. Task-specific ionic liquids as corrosion inhibitors on carbon steel in 0.5 M HCl solution: an experimental and theoretical study. *Corros. Sci.* **2019**, *153*, 301−313.
(41) Fekry, A. M.; Mohamed, R. R. Acetyl thiourea chitosan as an eco-friendly inhibitor for mild steel in sulphuric acid medium. *Electrochim. Acta* **2010**, *55*, 1933−1939.
(42) Arellanes-Lozada, P.; Díaz-Jiménez, V.; Hernández-Cocoletzi, H.; Nava, N.; Olivares-Xometl, O.; Likhanova, N. V. Corrosion inhibition properties of iodide ionic liquids for API 5L X52 steel in acid medium. *Corros. Sci.* **2020**, *175*, No. 108888.
(43) Fuchs-Godec, R.; Pavlović, M. G. Synergistic effect between non-ionic surfactant and halide ions in the forms of inorganic or organic salts for the corrosion inhibition of stainless-steel X4Cr13 in sulphuric acid. *Corros. Sci.* **2012**, *58*, 192−201.
(44) Hsu, C. H.; Mansfeld, F. Concerning the conversion of the constant phase element parameter Y0 into a capacitance. *Corrosion* **2001**, *57*, 747−748.
(45) Solomon, M. M.; Gerengi, H.; Kaya, T.; Kaya, E.; Umoren, S. A. Synergistic inhibition of St37 steel corrosion in 15% H_2SO_4 solution by chitosan and iodide ion additives. *Cellulose* **2017**, *24*, 931−950.
(46) Zheng, X.; Zhang, S.; Li, W.; Gong, M.; Yin, L. Experimental and theoretical studies of two imidazolium-based ionic liquids as inhibitors for mild steel in sulfuric acid solution. *Corros. Sci.* **2015**, *95*, 168−179.
(47) Onyeachu, I. B.; Obot, I. B.; Sorour, A. A.; Abdul-Rashid, M. I. Green corrosion inhibitor for oilfield application I: electrochemical assessment of 2-(2-pyridyl) benzimidazole for API X60 steel under sweet environment in NACE brine ID196. *Corros. Sci.* **2019**, *150*, 183−193.
(48) Sha, J.-Y.; Ge, H.-H.; Wan, C.; Wang, L.-T.; Xie, S.-Y.; Meng, X.-J.; Zhao, Y.-Z. Corrosion inhibition behaviour of sodium dodecyl benzene sulphonate for brass in an Al2O3 nanofluid and simulated cooling water. *Corros. Sci.* **2019**, *148*, 123−133.
(49) Abd El-Lateef, H. M.; Khalaf, M. M. Synergistic inhibition effect of novel counterion-coupled surfactant based on rice bran oil and halide ion on the C-steel corrosion in molar sulphuric acid: Experimental and computational approaches. *J. Mol. Liq.* **2021**, *331*, No. 115797.
(50) Lopes-Sesenes, R.; Dominguez-Patiño, G. F.; Gonzalez-Rodriguez, J. G.; Uruchurtu-Chavarin, J. Effect of flowing conditions on the corrosion inhibition of carbon steel by extract of buddleia perfoliata. *Int. J. Electrochem. Sci.* **2013**, *8*, 477−489.
(51) Ituen, E.; Akaranta, O.; James, A. Evaluation of performance of corrosion inhibitors using adsorption isotherm models: an overview. *Chem. Sci. Int. J* **2017**, *18*, 1−34.
(52) Wang, C.; Zou, C.; Cao, Y. Electrochemical and isothermal adsorption studies on corrosion inhibition performance of β-cyclodextrin grafted polyacrylamide for X80 steel in oil and gas production. *J. Mol. Struct.* **2021**, *1228*, No. 129737.
(53) Abd El Rehim, S. S.; Sayyah, S. M.; El-Deeb, M. M.; Kamal, S. M.; Azooz, R. E. Adsorption and corrosion inhibitive properties of P (2-aminobenzothiazole) on mild steel in hydrochloric acid media. *International Journal of Industrial Chemistry* **2016**, *7*, 39−52.
(54) Karthikaiselvi, R.; Subhashini, S. Study of adsorption properties and inhibition of mild steel corrosion in hydrochloric acid media by water soluble composite poly (vinyl alcohol-o-methoxy aniline). *J. Assoc. Arab Univ. Basic Appl. Sci.* **2014**, *16*, 74−82.
(55) Farag, A. A.; Hegazy, M. A. Synergistic inhibition effect of potassium iodide and novel Schiff bases on X65 steel corrosion in 0.5 M H2SO4. *Corros. Sci.* **2013**, *74*, 168−177.
(56) Kousar, K.; Walczak, M. S.; Ljungdahl, T.; Wetzel, A.; Oskarsson, H.; Restuccia, P.; Ahmad, E. A.; Harrison, N. M.; Lindsay, R. Corrosion inhibition of carbon steel in hydrochloric acid: Elucidating the performance of an imidazoline-based surfactant. *Corros. Sci.* **2021**, *180*, No. 109195.
(57) El-Mahdy, G. A.; Atta, A. M.; Al-Lohedan, H. A.; Tawfik, A. M.; Abdel-Khalek, A. A. Application of Silica/polyacrylamide nano-

composite as Anticorrosive layer for Steel. *Int. J. Electrochem. Sci.* **2015**, *10*, 151−161.
(58) Quadri, T. W.; Olasunkanmi, L. O.; Fayemi, O. E.; Solomon, M. M.; Ebenso, E. E. Zinc oxide nanocomposites of selected polymers: synthesis, characterization, and corrosion inhibition studies on mild steel in HCl solution. *ACS Omega* **2017**, *2*, 8421−8437.
(59) Morsi, R. E.; Labena, A.; Khamis, E. A. Core/shell (ZnO/polyacrylamide) nanocomposite: In-situ emulsion polymerization, corrosion inhibition, anti-microbial and anti-biofilm characteristics. *J. Taiwan Inst. Chem. Eng.* **2016**, *63*, 512−522.
(60) Tantawy, A. H.; Soliman, K. A.; Abd El-Lateef, H. M. Novel synthesized cationic surfactants based on natural piper nigrum as sustainable-green inhibitors for steel pipeline corrosion in CO2-3.5% NaCl: DFT, Monte Carlo simulations and experimental approaches. *J. Cleaner Prod.* **2020**, *250*, No. 119510.
(61) Adam, M. S. S.; Soliman, K. A.; Abd El-Lateef, H. M. Homodinuclear VO^{2+} and Ni^{2+} dihydrazone complexes: Synthesis, characterization, catalytic activity and CO_2-corrosion inhibition under sustainable conditions. *Inorg. Chim. Acta* **2020**, *499*, No. 119212.
(62) Farelas, F.; Ramirez, A. Carbon dioxide corrosion inhibition of carbon steels through bis-imidazoline and imidazoline compounds studied by EIS. *Int. J. Electrochem. Sci.* **2010**, *5*, 797.
(63) Amin, M. A.; Mohsen, Q.; Mostafa, N. Y.; Al-Refaie, A.; Bairamov, A. K.; Al-Maaesab, S.; Murillo, E. M.; Al-Qahtani, S. A. Case study: Impact of Amine Containing Organic Compound on the Corrosion and Electrochemical Behaviors of Constructive Alloys in Linear Alpha Olefin Environment. *Int. J. Electrochem. Sci.* **2014**, *9*, 7552−7573.
(64) Palaniappan, N.; Cole, I. S.; Kuznetsov, A. E. Experimental and computational studies of graphene oxide covalently functionalized by octylamine: electrochemical stability, hydrogen evolution, and corrosion inhibition of the AZ13 Mg alloy in 3.5% NaCl. *RSC Adv.* **2020**, *10*, 11426−11434.
(65) Lukovits, I.; Kálmán, E.; Zucchi, F. Corrosion Inhibitors—Correlation between Electronic Structure and Efficiency. *Corrosion* **2001**, *57*, 3−8.
(66) Yesudass, S.; Olasunkanmi, L. O.; Bahadur, I.; Kabanda, M. M.; Obot, I. B.; Ebenso, E. E. Experimental and theoretical studies on some selected ionic liquids with different cations/anions as corrosion inhibitors for mild steel in acidic medium. *J. Taiwan Inst. Chem. Eng.* **2016**, *64*, 252−268.
(67) Debab, H.; Douadi, T.; Daoud, D.; Issaadi, S.; Chafaa, S. Electrochemical and quantum chemical studies of adsorption and corrosion inhibition of two new Schiff bases on carbon steel in hydrochloric acid media. 2018, DOI: 10.20964/2018.07.19.
(68) Gao, G.; Liang, C. Electrochemical and DFT studies of β-amino-alcohols as corrosion inhibitors for brass. *Electrochim. Acta* **2007**, *52*, 4554−4559.
(69) Abd El-Lateef, H. M.; Shalabi, K.; Tantawy, A. H. Corrosion inhibition of carbon steel in hydrochloric acid solution using newly synthesized urea-based cationic fluorosurfactants: experimental and computational investigations. *New J. Chem.* **2020**, *44*, 17791−17814.
(70) Goyal, M.; Vashist, H.; Kumar, S.; Bahadur, I.; Benhiba, F.; Zarrouk, A. Acid corrosion inhibition of ferrous and non-ferrous metal by nature friendly Ethoxycarbonylmethyltriphenylphosphonium Bromide (ECMTPB): Experimental and MD simulation evaluation. *J. Mol. Liq.* **2020**, *315*, No. 113705.
(71) Oyebamiji, A. K.; Adeleke, B. B. Quantum chemical studies on inhibition activities of 2, 3-dihydroxypropyl-sulfanyl derivative on carbon steel in acidic media. *Int. J. Corros. Scale Inhib.* **2018**, *7*, 498−508.
(72) Hsissou, R.; Abbout, S.; Safi, Z.; Benhiba, F.; Wazzan, N.; Guo, L.; Nouneh, K.; Briche, S.; Erramli, H.; Touhami, M. E. Synthesis and anticorrosive properties of epoxy polymer for CS in [1 M] HCl solution: Electrochemical, AFM, DFT and MD simulations. *Constr. Build. Mater.* **2021**, *270*, No. 121454.
(73) Guo, L.; Safi, Z. S.; Kaya, S.; Shi, W.; Tüzün, B.; Altunay, N.; Kaya, C. Anticorrosive effects of some thiophene derivatives against the corrosion of iron: a computational study. *Frontiers in chemistry* **2018**, *6*, 155.
(74) Hsissou, R. Review on epoxy polymers and its composites as a potential anticorrosive coatings for carbon steel in 3.5% NaCl solution: Computational approaches. *J. Mol. Liq.* **2021**, *336*, No. 116307.
(75) Gece, G.; Bilgiç, S. Quantum chemical study of some cyclic nitrogen compounds as corrosion inhibitors of steel in NaCl media. *Corros. Sci.* **2009**, *51*, 1876−1878.
(76) Madkour, L. H.; Kaya, S.; Obot, I. B. Computational, Monte Carlo simulation and experimental studies of some arylazotriazoles (AATR) and their copper complexes in corrosion inhibition process. *J. Mol. Liq.* **2018**, *260*, 351−374.
(77) Shalabi, K.; Helmy, A. M.; El-Askalany, A. H.; Shahba, M. M. New pyridinium bromide mono-cationic surfactant as corrosion inhibitor for carbon steel during chemical cleaning: Experimental and theoretical studies. *J. Mol. Liq.* **2019**, *293*, No. 111480.
(78) Özcan, M.; Dehri, İ.; Erbil, M. Organic sulphur-containing compounds as corrosion inhibitors for mild steel in acidic media: correlation between inhibition efficiency and chemical structure. *Appl. Surf. Sci.* **2004**, *236*, 155−164.
(79) Ansari, K. R.; Chauhan, D. S.; Quraishi, M. A.; Mazumder, M. A. J.; Singh, A. Chitosan Schiff base: an environmentally benign biological macromolecule as a new corrosion inhibitor for oil & gas industries. *Int. J. Biol. Macromol.* **2020**, *144*, 305−315.
(80) Khodyrev, Y. P.; Batyeva, E. S.; Badeeva, E. K.; Platova, E. V.; Tiwari, L.; Sinyashin, O. G. The inhibition action of ammonium salts of O, O′-dialkyldithiophosphoric acid on carbon dioxide corrosion of mild steel. *Corros. Sci.* **2011**, *53*, 976−983.
(81) Ghareba, S.; Omanovic, S. Interaction of 12-aminododecanoic acid with a carbon steel surface: towards the development of 'green'corrosion inhibitors. *Corros. Sci.* **2010**, *52*, 2104−2113.
(82) Mazumder, M. A. J.; Al-Muallem, H. A.; Ali, S. A. The effects of N-pendants and electron-rich amidine motifs in 2-(p-alkoxyphenyl)-2-imidazolines on mild steel corrosion in CO2-saturated 0.5 M NaCl. *Corros. Sci.* **2015**, *90*, 68−54.
(83) Haddadi, S. A.; Ramazani, S. A. A.; Mahdavian, M.; Taheri, P.; Mol, J. M. C. Fabrication and characterization of graphene-based carbon hollow spheres for encapsulation of organic corrosion inhibitors. *Chem. Eng. J.* **2018**, *352*, 909−922.